New Optical and Near-Infrared Surface Brightness Fluctuations Models. II. Young and Intermediate Age Stellar Populations

Raimondo G.[1], Brocato E.[1], Cantiello M.[1,2], Capaccioli M.[3,4]

ABSTRACT

We present theoretical surface-brightness fluctuations (SBF) amplitudes for single–burst stellar populations of young and intermediate age ($25\,Myr \leq t \leq 5\,Gyr$), and metallicities $Z = 0.0003$, 0.001, 0.004, 0.008, 0.01, 0.02, and 0.04. The fluctuation magnitudes and colors as expected in the Johnson–Cousins (*UBVRIJHK*) photometric system are provided. We pay attention to the contribution of thermal–pulses asymptotic giant branch (TP–AGB) stars. The sensitivity of the predicted SBF to changes in the mass–loss scenario along the TP–AGB phase is examined. Below 0.6-1 Gyr both optical and NIR SBF models exhibit a strong dependence on age and mass loss. We also evaluate SBF amplitudes by using Monte Carlo techniques to reproduce the random variation in the number of stars experiencing bright and fast evolutionary phases (Red Giant Branch, AGB, TP–AGB). On this ground, we provide constraints upon the faintest integrated flux of real stellar populations required to derive reliable and meaningful SBF measurements.

We analyze a technique for deriving SBF amplitudes of star clusters from the photometry of individual stars, and estimate the indetermination due to statistical effects, which may impinge on the procedure. The first optical SBF measurements for 11 Large Magellanic Cloud (LMC) star rich clusters - with age ranging from few Myr to several Gyr - are derived by using Hubble Space Telescope observations. The measurements are successfully compared to our SBF predictions, thus providing a good agreement with models of metallicity $Z = 0.0001$–0.01. Our results suggest that, for TP–AGB stars, a mass loss

[1]INAF–Osservatorio Astronomico di Teramo, Via M. Maggini, I-64100 Teramo, Italy; raimondo@te.astro.it, brocato@te.astro.it, cantiello@te.astro.it

[2]Dipartimento di Fisica "E.R. Caianiello", Università di Salerno and INFN, Sezione di Napoli, Gruppo Collegato di Salerno, Via S. Allende, I-84081 Baronissi, Salerno, Italy

[3]Dipartimento di Scienze Fisiche, Università di Napoli Federico II, Complesso Monte S. Angelo, via Cintia, I-80126, Napoli, Italy; capaccioli@na.astro.it

[4]INAF–Osservatorio Astronomico di Capodimonte, via Moiariello 16, I-80131 Napoli, Italy

as a power-law function of the star luminosity is required in order to properly reproduce the optical SBF data of the LMC clusters. Finally, near–infrared models have been compared to available data, thus showing the general trend is well fitted. We suggest how to overcome the general problem of SBF models in reproducing the details of the near–infrared SBF measurements of the Magellanic Cloud star clusters.

Subject headings: (galaxies:) Magellanic Clouds — galaxies: star clusters — galaxies: stellar content

1. Introduction

Surface brightness fluctuations (SBF) technique (Tonry & Schneider 1988, TS88) is one of the most powerful methods to derive extragalactic distances of gas–free stellar systems. In the last decade, SBF were proven to be effective in estimating distances as far as 50 Mpc, and even larger, using ground–based observations (e.g. Tonry et al. 2001; Blakeslee, Vazdekis, & Ajhar 2001; Mei et al. 2001; Liu Graham & Charlot 2002), and out to distances exceeding 100 Mpc from the space (Pahre et al. 1999; Jensen et al. 2003). Since the method has been primarily applied to elliptical galaxies and to the bulges of spirals, theoretical SBF studies have been mostly oriented to old stellar systems ($t > 2$–$5\,Gyr$: Worthey 1993; Buzzoni 1993; Liu, Charlot, & Graham 2000; Blakeslee, Vazdekis, & Ajhar 2001; Cantiello et al. 2003).

Along with their ability in gauging distances, SBF appear to be a very promising tool for investigating the evolution of unresolved stellar populations in distant galaxies. Attempts have been made to derive consistent estimations of age and metallicity for samples of galaxies from SBF measurements (Brocato, Capaccioli & Condelli 1998; Liu, Charlot & Graham 2000; Blakeslee, Vazdekis, & Ajhar 2001; Liu, Graham, & Charlot 2002; Cantiello et al. 2003; Raimondo et al. 2004). However, even in galaxies dominated by old stars, disregarding the effect of the contribution by possible intermediate and young-age stellar populations ($t < 2$–$5\,Gyr$) may be a hazardous assumption. The presence of different stellar populations at different galacto-centric distances, revealed by integrated colors and spectral–indexes radial gradients, indicates that ellipticals are mostly composite stellar systems (e.g. Pagel & Edmunds 1981). SBF–gradient measurements support this view (Sodemann & Thomsen 1995; Cantiello et al. 2005). The presence of relatively young He–burning and/or AGB stars may contribute to the brightest part of the galaxy luminosity function (LF). Because the major contribution to the SBF signal comes from high luminosity stars, it is relevant to know how SBF amplitudes change by lowering the age of the stellar system down to a few million years, in those photometric bands where the SBF signal is mostly affected by the presence

of young and intermediate-age stellar populations.

Before facing the problem of age and metallicity of possibly mixed stellar populations in remote galaxies by using SBF, their capability as population tracer has to be proven and carefully tested on stellar systems of known distance, age, and metallicity. Then, once calibrated on resolved Galactic and Local Group stellar populations, SBF become a valuable tool in the analysis of the stellar content in galaxies, where crowding and distance hamper studies made with the classical color–magnitude diagram (CMD) technique.

SBF have also been recognized effective in constraining stellar evolution theory. In a previous paper (Cantiello et al. 2003, hereafter Paper I), we showed that SBF of old populations are sensitive to the number of very bright stars evolving along the early AGB, and thermally pulsating AGB (TP–AGB). In young stellar populations –old enough to stars in these stages– stochastic fluctuations of the number of AGB–stars (as triggered by mass–loss processes and evolutionary time-scale) is expected to have even more relevance in predicting SBF amplitudes. If this is confirmed, SBF can also provide a new and unexplored way for improving our understanding of physical processes at work in AGB stars of intermediate mass ($M \sim 5\,M_{\odot}$).

In the last few years, a large effort to improve stellar evolution models has been done in order to reproduce both the details of the AGB–stars evolution (Straniero et al. 1997; Pols at al. 2001), and the evolution of 'normal' stars. New physics experiments have advanced our knowledge of nuclear reactions rates inside stars, and the equation of state of stellar matter in critical conditions. Updated and homogeneous evolutionary–track databases, reproducing the observed CMD of young and intermediate–age stellar populations in detail (e.g. Brocato et al. 2003), are now available (Girardi et al. 2000; Castellani et al. 2003; Marigo et al. 2003; Pietrinferni et al. 2004). Therefore, very accurate SBF amplitudes can be computed now in this age range.

Pioneer work on SBF from young Simple Stellar Populations (SSPs) has been carried out by Gonzalez et al. (2003, 2004) in the near-infrared (NIR), and by Raimondo et al. (2003) in the optical regime. In the present paper, we evaluate SBF amplitudes expected from SSPs younger than $5\,Gyr$, with metallicities from $Z = 0.0003$ to 0.04. Much attention is devoted to a simulation of the TP–phase and its uncertainties, by evaluating changes of chemical composition, stellar temperature, and the whole structure of TP–AGB stars as prescribed by Wagenhuber & Groenewegen (1998, WG98). Mass–loss processes complicate enormously the modelling of TP–AGB stars observational properties.

This complex picture is expected to have a huge impact on the SBF behavior for intermediate–age stellar populations. In turn, SBF magnitudes and colors could be deci-

sive to put constraints on the evolution of AGB stars, e.g. the efficiency of mass-loss, in stellar systems with known age and metallicity, since they are extremely efficient in mapping the properties of very bright stars in the population (paper I).

In order to test our predictions, we select a sample of 11 star clusters of the Large Magellanic Cloud (LMC): for 7 such clusters the estimated age is within the range studied here; the others are as old as the Galactic Globular Clusters (GGCs). Optical SBF measurements are derived using the photometry of resolved stars from high resolution images of each cluster, as obtained with the Wide Field Planetary Camera 2 (WFPC2) on board of the Hubble Space Telescope (HST).

The paper is organized as follows. A description of inputs of the stellar population synthesis code is presented in Section 2. The methods for computing SBF amplitudes and stochastic effects, due to the number of stars in the population are presented in Section 3 and Section 3.1. SBF predictions are shown as a function of the TP–AGB stars mass–loss rate in Section 3.2, and metallicity in Section 3.3. We derive the optical SBF measurements of the LMC star clusters in Section 4, and present the relative comparison with models in Section 5, together with a discussion on NIR SBF. A summary and final conclusions end the paper (Section 6).

2. Theoretical Framework

In order to compute SBF amplitudes, we use the stellar population synthesis code, described in Brocato et al. (1999, 2000). Here, we only recall that the code starts directly from stellar evolutionary tracks and relies on the Monte Carlo technique for populating the Initial Mass Function (IMF). The former property avoids any problem in the mass–bin or luminosity–bin procedures, which may affect the use of isochrones. The latter property allows us to take into account stochastic effects, due to the number of stars in the stellar system, even for SBF amplitudes. If we deal with star clusters and under–sampled stellar systems, stochastic fluctuations of the number of bright stars may affect integrated quantities (e.g. Santos & Frogel 1997; Brocato et al. 1999). The procedure used here takes directly into account these effects.

The present SSP models rely on the evolutionary–track database by Pietrinferni et al. (2004, P04). All the evolutionary phases, from the Main Sequence (MS) up to the AGB, are covered by models. In particular, the AGB evolution runs up to the onset of the first thermal pulse or to the carbon ignition. We selected stellar evolutionary models with metallicities $Z = 0.0003, 0.001, 0.004, 0.008, 0.01, 0.02$, and 0.04, computed by adopting a solar–scaled

metal distribution with an enrichment law of $\Delta Y/\Delta Z \simeq 1.4$.

In spite of the numerous improvements in the accuracy and precision of stellar evolutionary models, only a few tracks provide a detailed and full evolution along the TP–AGB phase (e.g. Straniero et al. 1997; Herwig et al. 1997; Pols at al. 2001). Moreover, not all of them cover homogeneously a wide range of chemical compositions and stellar masses, needed to investigate resolved and unresolved stellar populations. Since bright stars play a relevant role in determining SBF, the TP–AGB phase cannot be neglected. We devoted a particular care in including this evolutionary phase in our simulations. For the sake of readability, the discussion and details on how we threat TP–AGB stars are presented in Appendix A.

In the present paper, color–effective temperature (T_{eff}) relations come from the semi–empirical compilation by Westera et al. (2002), which is an updated version of the library by Lejeune et al. (1997). A Scalo–like IMF (Scalo 1998) is assumed for stellar masses in the interval $m = 0.1$–$10\,M_{\odot}$. Note that the upper mass limit corresponds to the highest mass evolving off the MS in the youngest population we considered, i.e. $t \sim 25\,Myr$. All the more massive stars are expected to be exploded as supernovae, since their quiescent nuclear burning life-time is as long as a few million years.

By means of Monte Carlo techniques, $N_{sim} = 5000$ *independent* simulations are computed for each set of SSP parameters, i.e. age (t), and metallicity (Z). The total mass of each simulation is typically $\mathcal{M} \simeq 10^4\,M_{\odot}$, unless explicitly stated otherwise. The explored age range is $25\,Myr \leq t \leq 5\,Gyr$[1]. As an example of one of the 5000 simulations, in Fig. 1 we report the synthetic CMDs of the simulated stellar populations – for few selected ages – in the theoretical $log\ L/L_{\odot}\ vs.\ log\ T_{eff}$ plane.

3. SBF Amplitudes

In this section, we present two different methods for computing SBF. We discuss in detail their analogies with observations, and investigate stochastic effects on SBF amplitudes, caused by the discrete nature of the number of stars in stellar systems. The impact of bright and rare TP–AGB stars on SBF is also presented.

The *standard* procedure we developed to calculate SBF is already presented in Paper I (*std*–procedure). It is based on the following equation, valid in the *gaussian statistics* regime,

[1]At the time of publication, models fully consistent with the present theoretical scenario for ages larger than $5\,Gyr$, and for all metallicities presented here are available at the web site: www.te.astro.it/SPoT. These old–age models will be discussed in detail in a forthcoming paper.

i.e. high number of stars (TS88):

$$\overline{M}_X = -2.5\, log\, \overline{F}_X = -2.5\, log\, [\frac{\langle (\, F_X - \langle F_X \rangle)^2 \, \rangle}{\langle F_X \rangle}] \tag{1}$$

where $\overline{F}_X$ is the fluctuation flux in the generic photometric filter X; F_X and $\langle F_X \rangle$ are respectively the total flux of each simulation, and the mean total flux averaged over N_{sim} simulations, i.e.:

$$F_X \equiv F_X^j = \sum_{i=1}^{N_{star}} f_i(X) \qquad j = 1, N_{sim} \tag{2}$$

$f_i(X)$ corresponds to the absolute flux of the i-th star populating the j-th simulation, and

$$\langle F_X \rangle = \frac{\sum_{j=1}^{N_{sim}} F_X^j}{N_{sim}} \tag{3}$$

For the sake of clarity, in this section absolute SBF amplitudes derived from Eq. 1 are called *standard*–SBF, and indicated as $\overline{M}_X^{std}$. As quoted in Paper I, there is a close correspondence between the *std*–procedure and the way of measuring SBF for unresolved stellar populations. In fact, the integrated energy flux F_X^j corresponds to the flux measured in a single pixel of a galaxy CCD image (if both seeing and population mixture are neglected).

When N_{sim} is equal to 5000, $\overline{M}_X^{std}$ is called *asymptotic value* ($\overline{M}_X^{std,asym}$). Note that $\overline{M}_X^{std}$ runs very quickly (after few hundreds of simulations) towards $\overline{M}_X^{std,asym}$ (Appendix B), and the uncertainties are reduced ($\simeq 0.05\, mag$, Paper I). The *asymptotic* value has the same physical meaning of the classical SBF predictions in the literature (e.g. Worthey 1993; Buzzoni 1993; Liu, Charlot, & Graham 2000; Blakeslee, Vazdekis, & Ajhar 2001, G04).

For spatially-resolved star clusters, we can apply another technique for measuring SBF. It was first introduced by Ajhar & Tonry (1994, AT94), and is based on individual–star photometry. By means of our method of computing SSP models and integrated properties, we can provide SBF predictions for each j-th simulation, by directly applying the definition of SBF, as introduced by TS88 (Eq. 7-9):

$$\overline{M}_X^{RS,j} = -2.5 \log\, [\frac{\sum_{i=1}^{N_{star}} f_i(X)^2}{\sum_{i=1}^{N_{star}} f_i(X)}] \qquad j = 1, N_{sim}. \tag{4}$$

Note that $\overline{M}_X^{RS,j}$ corresponds to the SBF obtained using the photometry of all stars in a cluster, and directly relies upon the *poissonian statistics*. The mean SBF magnitude

averaged over $N_{sim} = 5000$ independent simulations is:

$$\overline{M}_X^{RS} = \frac{\sum_{j=1}^{N_{sim}} \overline{M}_X^{RS,j}}{N_{sim}}, \tag{5}$$

and the SBF statistical uncertainties can be derived as the standard deviation of the $\overline{M}_X^{RS,j}$ distribution. In the following, this procedure for computing SBF is indicated as *RS*–procedure (Resolved Systems).

3.1. Statistical Effects

In principle, the two procedures should provide very similar results. In practice, this is only true if the number of stars included in the j-th simulation is large enough to populate all the evolutionary phases (i.e. the poisson statistics coincides with the gaussian one, TS88; Paper I). Hence, in order to analyze star clusters SBF magnitudes, and to properly compare models with observations, it is crucial to investigate the dependence of SBF amplitudes upon quantities related to the number of stars in the population. In the following, we present a careful analysis of the statistical effects on SBF predictions. Although the analysis is specifically performed for star clusters, the technique we developed can be applied to any spatially resolved populations.

For fixed age and metallicity, variations of the total number of stars among clusters result in a variation of the cluster total V–magnitude (M_V^{tot}). This is an observational quantity related to the number of stars included in the stellar population. We computed SBF amplitudes, by adopting both procedures (*std*–procedure: Eq. 1; and *RS*–procedure: Eq. 5), by varying the SSP integrated absolute magnitude (M_V^{Tot}) from $M_V^{Tot} \simeq -1$ to $-11\,mag$, a range larger than that observed for LMC clusters. This corresponds to varying the total mass of the population from $\mathcal{M}_{tot} \sim 10^2$ to $\sim 10^5 M_\odot$. As usual, for each set of parameters (t, Z) we computed N_{sim} *independent* simulations.

Fig. 2 shows the behavior of $\overline{M}_X^{std,asym}$ in the V, I, and K bands as a function of M_V^{Tot} (solid thick line, open circles). Models for three different ages $t = 100\,Myr$, $t = 900\,Myr$, and $t = 3\,Gyr$, and $Z = 0.008$ are displayed. From all the panels, it is evident that *asymptotic* SBF amplitudes ($\overline{M}_X^{std,asym}$) are stable within $0.1\,mag$ in the wide range of M_V^{Tot}. In other words, independently of the cluster mass (luminosity), fluctuation amplitudes computed over 5000 simulations with the *std*–procedure predict nearly constant values.

SBF amplitudes resulting from the *RS*–procedure ($\overline{M}_X^{RS}$) are plotted as filled circles in Fig. 2. The uncertainties due to stochastic fluctuations of the number of bright stars are

directly evaluated as the standard deviation of the $\overline{M}_X^{RS}$ distribution, and plotted as 1 σ error-bars. It is worth noting that the $\overline{M}_X^{RS}$ *versus* M_V^{Tot} behavior is similar to that shown by integrated colors (e.g. Santos & Frogel 1997; Brocato et al. 1999).

The difference between the SBF *asymptotic* value and that derived from Eq. 5 is larger in NIR bands than in blue bands, because in the optical bands the contribution of the sparsely populated RGB and AGB is less important than that of the well populated MS. By increasing the total luminosity (i.e. increasing SSP mass), the two procedures converge to the same SBF value, and the uncertainty due to stochastic effects decreases accordingly. This happens when each simulation is well populated in all post–MS evolutionary stages until the TP–phase. The maximum value of M_V^{Tot} ($M_V^{Tot,max}$), where the two procedures give the same results –within uncertainties– slightly depends on the age, in the sense that the older the population, the fainter is $M_V^{Tot,max}$. It changes from $M_V^{Tot,max} \simeq -6.5$ to $-4.5\,mag$ by varying the age from $t = 100\,Myr$ to $3\,Gyr$.

Since the two theoretical procedures reflect different ways of measuring SBF, the last finding has direct effects upon the observations. The condition $M_V^{Tot} \lesssim M_V^{Tot,max}$ must be satisfied when comparing classical (*asymptotic*) SBF predictions to measurements derived from single–star photometry. In relatively poorly populated stellar systems, the random occurrence of bright stars deeply affects the SBF, and should be taken into account in the comparison with models (that is $\overline{M}_X^{RS}$ should be preferred).

In the *std*–procedure (i.e. the one applied to measure SBF in galaxies) SBF are derived by using the integrated flux of a large number of 'similar' but 'uncorrelated' populations (i.e. 'similar' but 'uncorrelated' pixels). This ensures the *asymptotic* SBF value is reached even taking into account a relatively small number of pixels (see Appendix B). For example, if a fraction of young populations is expected in a galaxy, simulations suggest that the effective number of pixels used in measuring SBF should not be less than 2000, so as to reduce the uncertainties due to statistical effects. This constraint becomes less stringent if the mass density of the young population is larger than $\gtrsim 10^4\,M_\odot$/pixel, i.e. 500 pixels are expected to be enough to keep such uncertainties below $0.1\,mag$.

In conclusion, we find that SBF models (classical asymptotic models) well represent SBF as observed in galaxies, while SBF measured from resolved stellar systems require caution before performing comparisons with models. In particular, when comparing SBF predictions with SBF observations for star clusters or under–sampled stellar populations, attention should be payed in taking into account uncertainties due to the stochastic occurrence of bright stars experiencing fast and luminous evolutionary phases.

3.2. The impact of TP–AGB stars

Being extremely bright and rare, TP–AGB stars are relevant in determining SBF of young/intermediate–age stellar populations. One of the processes which triggers the luminosity and the duration of the TP-phase is mass–loss. There are different mass–loss scenarios to be adopted along the TP–phase (see Appendix A for a detailed discussion). This is a critical assumption, because the mass–loss efficiency determines the number of very bright TP–AGB stars. In order to understand the effective (quantitative) impact of such stars on SBF, we computed a set of models by varying only the mass–loss rate:

BH–models: *mild* mass–loss rate (Baud & Habing 1983, hereafter BH), the TP–phase is well populated (Eq. A7) ;

$B1$–models: *moderate* mass–loss rate (Blocker 1995, hereafter B95), few stars in the TP–phase (Eq. A8);

$B2$–models: *high* mass–loss rate (B95), few stars in the TP–phase (Eq. A9);

no–TP models: *huge* (unreal) mass–loss rate, no stars in the TP–phase.

Let us analyze the case of $Z = 0.008$, i.e. a metallicity expected to be representative of young/intermediate LMC star clusters (Westerlund 1997) we shall use as observational counterparts in Section 4. Fig. 3 illustrates the time evolution of SBF predictions for the four assumptions of mass–loss rate. We find that SBF in the U, B, and V bands are not significantly affected by TP–AGB stars mass–loss processes. Whereas, for redder bands, from R to K, SBF may change by more than $1\,mag$ for models older than $\sim 50\,Myr$ and younger than $\sim 1\,Gyr$. The former value corresponds to the appearance of the AGB in an SSP of such a metallicity (AGB–phase transition); the last one is related to the appearance of the RGB (RGB–phase transition, Renzini & Buzzoni 1986). In this age–range, the cool AGB (including TP–AGB) stars dominate the integrated bolometric light.

In *no–TP* models, the brightest objects in the SSP are early–AGB stars, i.e. stars before the first thermal pulse. Thus, SBF amplitudes are less luminous and extremely sensitive to the appearance of the RGB. On the other hand, BH mass–loss rate is not very efficient, and the resulting relatively high number of TP–stars has three consequences: i) SBF are the most luminous (within our four cases) at any age, ii) SBF experience an evident jump, due to the occurrence of the AGB phase–transition at $t \sim 50\,Myr$, and iii) SBF do not vary significantly at the RGB–phase transition age. $B1$– and $B2$–models lie within the previous two extreme cases. Since $B1$ and $B2$ mass–loss rates exponentially depend upon the star luminosity, mass loss is much more efficient in massive AGB stars (young SSPs, $t \lesssim 200\,Myr$) than in low–mass AGB stars (old SSPs). Consequently, in young SSPs, the TP–phase is less

populated, thus bringing the SBF values toward the *no–TP* case.

For ages $t \gtrsim 1\,Gyr$ AGB stars become less relevant in predicting SBF, because the RGB tip is nearly as bright as the AGB tip, but much more populated (of about a factor 10). This is the main reason why the four curves appear to converge at older ages.

Fluctuation colors present a very similar behavior (Fig. 4), showing a high sensitivity to TP–AGB stars mass–loss rate and to the phase–transitions. Of course, SBF colors might be more effective for detecting the efficiency of TP–AGB stars mass–loss rate than fluctuation magnitudes, as a consequence of their independence from distance.

The results in Fig. 3 and Fig. 4 suggest at least two considerations: *a*) indications on the age of distant stellar systems can be inferred by measuring SBF in blue bands (U, B and V); and *b*) SBF measured in single–burst stellar populations would provide a tool to quantitatively evaluate the properties of TP–AGB stars, e.g. the expected number, luminosity, and their mass loss.

3.3. SBF versus Metal Content

Before concluding this Section, we discuss the SBF dependence on the chemical composition. Table 1 and Fig. 5 report SBF amplitudes in Johnson–Cousins bands for different chemical compositions as a function of age. The input assumptions are the same as quoted at the beginning of this section, and the adopted mass–loss scenario is $B1$. The reason of this choice is given in Section 4. Table 1 lists: age (Col. 1), absolute SBF magnitudes in various photometric filters (Cols. 2–10), absolute integrated V magnitude and $V-I$ integrated color of the population (Cols. 11–12). The SBF predictions are available at the web–site: http://www.te.astro.it/SPoT.

The general trend of SBF magnitudes at different chemical compositions is similar to the one shown by models with $Z = 0.008$. As a general indication, we find that metal–poor ($Z \lesssim 0.001$) SSPs tend to have brighter SBF in the optical bands. It is the opposite for NIR bands, since metal–rich populations show brighter SBF, especially at an old age. This can better understood if we remember that the RGB and AGB of metal–rich stars are cooler than the corresponding branches of metal–poor stars. Moreover, at young ages (several Myr) the appearance of AGB stars causes a sudden jump in the *mean* NIR–SBF magnitude/color of the population. This is because SBF are an extremely efficient measure of any fluctuation of the distribution of bright stars in the population. Since metal–rich (pre-AGB) bright stars are typically *redder* than similar metal–poor stars, correspondingly, the appearance of AGB stars is expected to produce a less intense variation in the NIR SBF of a metal–rich

population.

Looking at both Fig. 3 and Fig. 5, one can note that the strong dependence of NIR SBF on mass loss, especially for intermediate–age populations, has several implications. The NIR SBF with intermediate mass–loss (B1) can look similar to those with mild mass–loss (BH), depending on metallicity. This behavior might generate a possible problem of degeneracy, when the metallicity of the stellar system is unknown. In addition, the evidence that mass loss increases with metallicity in AGB stars (Groenewegen et al. 1995) might complicate the scenario. On the other hand, this high sensitivity can be used to discriminate among different mass–loss assumptions, if stellar systems with known metallicity are considered, thus making SBF an interesting tool for investigating properties of AGB stars. In Section 4, we shall use WFPC2/HST SBF data to discriminate the mass–loss scenario, active in TP–AGB stars, for a sample of LMC star clusters.

4. SBF Measurements

To our knowledge, optical–SBF models available in the literature do not include predictions for young stellar populations, as they usually extend down to 2–5 Gyr (Worthey 1993; Buzzoni 1993; Liu, Charlot, & Graham 2000; Blakeslee, Vazdekis, & Ajhar 2001; Paper I). Thus, no comparison with optical SBF–models from other authors can be done. In this Section, we provide the first step toward the measure of optical SBF for young simple stellar systems.

Stellar clusters in the Magellanic Clouds (MC) represent a unique opportunity to explore the behavior of SBF in young and intermediate–age stellar systems. The MC clusters – formed at different epochs– provide a remarkable sampling of stellar clusters in a wide range of ages. Moreover, because of their proximity, they allow us to perform direct photometry of individual stars. This is of paramount importance in probing stellar population synthesis tools and models. The criteria for selecting MC star clusters, as well as photometric data analysis, are two important steps in our overall investigation. Hence, in the following section, we describe these steps in detail before discussing the SBF measurements.

4.1. Star clusters and photometric data selection

As shown in Section 3.1, the low statistic in the brighter part of the cluster luminosity function (LF) plays a role in determining the uncertainties of the measured SBF. For this reason, we prefer clusters with a number of stars high enough to avoid large statistical

fluctuations (Fig. 2). While taking this condition into account, we give the priority to more massive clusters, by selecting LMC young clusters, whose integrated magnitudes satisfy the condition $M_V^{Tot} \lesssim M_V^{Tot,max}$ at any age.

An accurate photometry of individual stars in the cluster core is another crucial requirement in order to fully map all the features of the cluster stellar population. We take advantage of the WFPC2/HST high capability of resolving stars in the core of the MC clusters. Mackey & Gilmore (2003, MG03) have shown that the core radius of MC clusters is typically smaller than $30''$, thus the WFPC2 field of view is large enough to contain most stars in the cluster.

With a total apparent magnitude $V^{Tot} = 9.89 \pm 0.01$ (van den Bergh 1981), NGC 1866 is one of the most massive cluster formed in the LMC during the last $3\,Gyr$. Our group has recently obtained deep and accurate WFPC2/HST observations in the $F555W$ ($\sim V$) and $F814W$ ($\sim I$) filters of this cluster (Walker et al. 2001; Brocato et al. 2003). Hence, it is a good candidate for our purpose. Further, we select a sample of LMC clusters spanning the age range from a few million up to a few billion years, for which similar HST observations in the same photometric filters are available. A sub–sample of the LMC clusters studied by de Grijs et al. (2002a, 2002b, 2002c) satisfy most requirements, namely: NGC 1805, NGC 1818, NGC 1831, NGC 1868, NGC 2209 and $Hodge$ 14. Their observations, just like our own for NGC 1866, reach magnitudes as faint as $V \sim 25\,mag$. Moreover, de Grijs and collaborators could detect radial mass segregation in the central regions of these LMC clusters. This is a clear indication of the high level of completeness and accuracy of their photometric data and LFs.

In order to minimize possible differences in handling the data, the original images have been retrieved from the HST archive, and analyzed by following the same procedure - discussed in Brocato et al. (2003), and briefly described here. The basic information on the images we used are summarized in Table 2. Each frame has been pre–processed according to the standard WFPC2 pipeline, by using the latest available calibrations. The removal of cosmic rays and the photometry have been performed by using the most recent version of the HSTphot package developed by Dolphin (2000a). The Point Spread Function (PSF) fitting option on the HSTphot routine has been adopted in order to take advantage of the PSFs, which are computed directly to reproduce the shape details of star images as obtained in the different regions of the WFPC2. Charge Transfer Efficiency (CTE) corrections and calibrations to the standard VI system were obtained directly by HSTphot routines, as documented by Dolphin (2000b). In Fig. 6 the resulting CMDs are plotted, together with the typical uncertainties on the photometry as a function of magnitude. The V and I photometry of de Grijs and collaborators are compared with the present work. The agreement is

extremely good, being the mean differences of the order of a few hundreds of magnitudes in all the chips, and for all the clusters. Completeness has been evaluated by distributing artificial stars of known positions and magnitudes, in selected circular regions around the cluster center. Since the resulting completeness functions strictly agree with those published by de Grijs et al. (2002a, 2002c, see their Fig. 2), we do not present nearly identical figures.

Even if the present paper is mainly devoted to young stellar clusters, for the sake of completeness we also added four really old clusters. We derived $\overline{V}$ and $\overline{I}$ also for NGC 1754, NGC 1916, NGC 2005, and NGC 2019, by relying on the high quality and deep HST photometry by Olsen et al. (1998), who used deep exposures in both $F555W$ and $F814W$ filters. This assures to measure stars of $V \sim 25$, well below the MS TO point for all the clusters.

Finally, we have a sample of 11 LMC star clusters. The complete list and a few properties of the clusters are presented in Table 3: cluster name (Col. 1); total V–magnitude from van den Bergh (1981), and present work (Cols. 2, 3); $\overline{V}$, $\overline{I}$, and $\overline{V} - \overline{I}$ (Cols. 4-6); Col. 7 lists cluster age as derived in Section 4.3 or from the literature (references in Col. 8). The uncertainties of SBF data refer to the maximum/minimum SBF values obtained by including field contamination and 'missed' bright stars, as described in the following section. The integrated magnitudes obtained in the present work refer to the photometric data used to derive the SBF measurements. They agree with values of van den Bergh (1981) within few tenths of magnitudes. For *Hodge* 14 the difference is larger, due to the severe area selection we used in order to minimize the field contamination (see the following section).

4.2. Optical SBF

In order to measure SBF, we followed the procedure described by AT94, by means of the photometry of individual stars in the cluster. Stars 8-10 *mag* fainter than the brightest stars of the cluster have been measured through high–resolution WFPC2 imaging. This allows us to use individual stars photometry not only to evaluate the numerator in Eq. 4, but also the denominator without introducing other sources of uncertainty in estimating the total flux (e.g. sky–level evaluation). Differently from the present work, AT94 (and G04) were forced "...to sum the flux of the CCD image with the sky subtracted..." to account for the contribution of the large number of unmeasured faint stars to the total flux. This is due to the fact that the photometry used in those papers does not reach the faint part of the MS (see e.g. the case of 47 Tuc in Fig. 10 of AT94).

The faint magnitude limit of the photometry is a crucial point in evaluating the denominator of Eq. 4, as enlightened by AT94. In order to find a quantitative indication of the im-

pact of faint MS stars on SBF, we used the following procedure. First, the VI SBF are derived from synthetic VI CMDs, containing stars with masses down to $M = 0.1\,M_{\odot}$, by applying the RS–procedure (Eq. 4). Then, the SBF are re-computed by artificially cutting out stars with $V > V_{cut}$ from the complete synthetic CMDs for a selected set of V_{cut}. This test corresponds to a simulation of 100% incompleteness at magnitudes fainter than V_{cut}. The V and I bands SBF have been derived by adopting the LMC absolute distance modulus $(m - M)_0 = 18.4 \pm 0.1$, and mean reddening $E_{B-V} = 0.06$ (Walker et al. 2001; Alcock et al. 2004). The procedure has been repeated for three different populations aged: $t = 100\,Myr$, $900\,Myr$, and $4\,Gyr$. The differences between the SBF derived by considering the complete synthetic CMDs and those from the 'cutted' ones are presented in Fig. 7 as a function of V_{cut}. The figure shows that the younger is the cluster, the brighter is the completeness limit required to minimize the difference between SBF computed by including all stars of the CMD, and SBF obtained by including only stars with $V < V_{cut}$. For clusters as old as $t = 4\,Gyr$, the uncertainty of SBF introduced by incompleteness is $\leq 0.2\,mag$ in $\overline{V}$, and $\leq 0.03\,mag$ in $(\overline{V} - \overline{I})$ if $V_{cut} \geq 23\,mag$. For clusters younger than $\sim 900\,Myr$ the uncertainty of SBF keeps below $0.2\,mag$ in $\overline{V}$, and $\lesssim 0.05\,mag$ in $(\overline{V} - \overline{I})$ if $V_{cut} \geq 21\,mag$.

As regards the LMC clusters considered here, the completeness of NGC 2209 and $Hodge\,14$ is shown to be larger than 90% for V and $I \leq 23$, while for younger clusters (NGC 1805, NGC 1818, NGC 1831, NGC 1866, NGC 1868) it is larger than $\sim$ 80–90% for V and $I \lesssim 21$ except for the innermost annulus, i.e. $r \leq 3.6''$ (de Grijs et al 2002a, 2002c; Brocato et al. 2003). As for old clusters (NGC 1754, NGC 1916, NGC 2005, and NGC 2019), we used the photometric data by Olsen et al. (1998), who made deep exposures in both $F555W$ and $F814W$ filters. This allows us to reach $V \sim 25\,mag$, well below the MS–TO point. Again, for all these clusters completeness at $V \leq 23\,mag$ is assured to be more than 80% for $r \geq 5''$.

Thus, the uncertainty of $\overline{V}$ and $\overline{I}$ due to the incompleteness is very small, well–below $0.2\,mag$ for all the ages considered. This ensures that $\overline{V}$ and $\overline{I}$ are derived with a degree of precision adequate for the level of intrinsic uncertainty due to statistical fluctuations expected for LMC clusters (Section 3.1).

Crowding effects might also be relevant in evaluating the numerator of Eq. 4. The technique of distributing artificial stars also helps in studying this issue. From Fig. 2 by de Grijs et al. (2002c) it is evident NGC 1831, NGC 1868, NGC 2209 and $Hodge\,14$ are not affected by crowding effects showing a $\sim$ 100% completeness for the 3 brightest magnitudes of the cluster stars. A similar evidence can be derived for NGC 1866 (Brocato et al. 2003). On the other hand, NGC 1805 and NGC 1818 may suffer a 10% of missed stars within $7.2''$ from the center (representing less than 3.5% of the PC area). Since the completeness functions

have a statistical meaning, a single young cluster has been further analyzed in order to check whether very bright stars are missed due to crowding effects and/or saturation problems. For clusters younger than a few billion years, we must pay a particular attention to bright and cool AGB stars, which may strongly affect the SBF measurements. In order to check the completeness of the brightest end of the LF, we retrieved for each cluster the images and the JHK_s photometry available in the Final Release of the Two Micron All Sky Survey (2MASS)[2]. Then, a star by star cross–identification between the two sets of photometry (HST and 2MASS) has been performed to avoid cool AGB stars within the observed field could be missed in the final photometric list used to derive SBF. If we missed one or more cool stars in the HST photometry, their corresponding V and I magnitudes have been obtained from the literature. The V and I magnitudes of such bright and cool AGB stars are available in the literature, mainly because of the large efforts done in the past in searching AGB carbon–rich stars (C–stars) in the LMC clusters (e.g. Aaronson & Mould 1982, Westerlund et al. 1991).

However, there is no guarantee that such bright stars found within the observed cluster field all belong to the cluster. For this reason, we provide – as an indicative uncertainty of the SBF measurements – half the difference between the SBF, computed by using only stars within the PC field, and the SBF obtained by adding to the photometric list the *missed* bright stars. This is a safe assumption, which probably leads to overestimate the uncertainty. Nevertheless, the primary goal of this paper is to explore the general behavior of optical SBF of young stellar populations, while leaving a detailed and quantitative analysis on LMC clusters to a forthcoming paper.

In the data analysis we also looked for another severe effect of crowding, that is the blending effect. The completeness curves we considered are corrected for it as well as for superposition of multiple randomly placed artificial stars. However, to make a further check, we estimated the number of expected blended pairs as discussed by Stephens et al. (2001). Dealing with WFPC2/HST, even in the worst case of a very densely populated core of a cluster like NGC 1866, the number of blended pairs formed by two identical giant stars is estimated to be of the order 0.0001% for the PC, and about 0.01% for the WF chips.

The field stars contamination is not severe for the selected clusters (with the exception of *Hodge* 14). The contribution of field stars on SBF measurements is evaluated by comparing SBF magnitudes derived from the whole region covered by the WFPC2 with the results obtained from the PC area only, which typically includes most of the stars of the cluster.

Finally, the four truly old clusters show SBF magnitudes in very good agreement with the average SBF values obtained for the GGCs by AT94. This last point can be also seen

[2]http://www.ipac.caltech.edu/2mass/

as *a posteriori* verification that our method of measuring SBF from high quality and deep photometric data is reliable, at least for the purpose of the present paper.

4.3. Age Determination

We used present synthetic CMDs to consistently evaluate the age of each cluster. In Fig. 6 we show the comparison between the observed CMDs and the synthetic ones. For all the clusters, we assumed a metallicity equal to $Z = 0.008$ and an absolute distance modulus of $(m-M)_0 = 18.4 \pm 0.1$. The reddening value of each cluster is derived from the best–fitting procedure as discussed in Walker et al. (2001). The assumed distance to the LMC appears justified in the light of recent distance measurements, which attempt to reconcile the long– with the short–distance scale (e.g. Salaris et al. 2003; Alcock et al. 2004).

The cluster age and the related overall uncertainty is reported in Table 3 (Col. 7). They are in good agreement with ages listed by MG03. The interstellar reddening values fall within the range measured for the LMC, e.g. $E_{B-V} = 0.06$–0.20 (Westerlund 1997).

Fig. 6 confirms the extremely high degree of accuracy that our SSP models reach in simulating the CMDs of young stellar populations. On the other side, we remark that our procedure is fully consistent, since the same theoretical framework was adopted for computing SBF, and for the CMD–analysis aimed to obtain the age of each cluster.

5. Models vs. Observations

5.1. Optical SBF

In this Section, we compare SBF predictions with the optical measurements. As discussed in Section 3.2, the $(\overline{V} - \overline{I})$ fluctuation color is sensitive to the mass–loss rate, active along the final stages of the AGB. In Fig. 8 observational data for clusters with age $t < 5\,Gyr$ are located within the two theoretical curves representing models *without* TP–AGB stars (no–TP, dotted line), and models computed by assuming the BH mass–loss rate (solid line). The cluster $Hodge\,14$ is the only exception: we shall discuss it later. Being the less efficient rate explored in the present work, the BH mass–loss rate predicts a large number of TP stars which are responsible for very 'red' $(\overline{V} - \overline{I})$ colors of young SSPs. In spite of the large error–bars of the LMC clusters data, Fig. 8 suggests that $B1$– and $B2$–models give a better fit than BH–models for nearly all the clusters. In particular, NGC 1866, for which we succeed in minimizing the uncertainties, is well fitted by models with mass–loss prescriptions

by B95.

In the same figure, old and very metal–poor models ($t > 5\,Gyr$, $Z = 0.001$ and 0.0001) published in Paper I are plotted as three/four–pointed stars. They have been computed by assuming a Reimers mass–loss rate (see Paper I for details). Note that, models of age $t > 5\,Gyr$ fully consistent with the present theoretical scenario will be discussed in a forthcoming paper (see note 5).

Fig. 9 exhibits the $\overline{M}_V$ and $\overline{M}_I$ behavior with age. For $t < 5\,Gyr$ we plot SBF models of all the metallicities presented in the present paper; $B1$ mass–loss scenario is taken only. For older ages, models with $Z = 0.001$ and $Z = 0.0001$ are taken from Paper I. The theoretical SBF refer to the asymptotic values (*std*–procedure) for which the indetermination is of the order of $0.05\,mag$ as already discussed. We also evaluated the *intrinsic* uncertainty due to stochastic effects on the number of bright stars (*RS*–procedure) from the models with the faintest M_V^{tot} (Table 1). According to the discussion in Section 3.1, the fainter is the integrated V magnitude of the cluster, the larger is the *intrinsic* uncertainty. We finally find out that it is of the order of $0.2\,mag$.

The general trend of $\overline{M}_V$ for LMC clusters is well reproduced by models in the explored age range (Fig. 9*a*). The SBF measurements of clusters younger than $5\,Gyr$ appear in agreement with models of metallicities $Z = 0.004 - 0.01$, which are appropriate for young and intermediate LMC clusters (e.g. Westerlund 1997; MG03). SBF measurements for very old clusters are fitted by 12–15 Gyr with a lower metallicity models.

For I-band SBF (Fig. 9*b*) the agreement is still good in the case of measurements with small uncertainties. Some relevant discrepancies arise for NGC 1868, NGC 2209, and $Hodge\,14$. Let us recall that the three quoted clusters have the faintest integrated light in our sample, thus statistical effects may be not negligible as inferred from Fig. 2 (Section 3.1). We also remind the reader that, in order to avoid contamination by field stars, in the case of $Hodge\,14$ a small fraction (i.e. a small mass) of the cluster is being analyzed only. This indication is confirmed if detailed models are computed by assuming exactly the integrated magnitude, and age reported in Table 3 (Col. 3, 7). The I–band SBF, derived by applying the *RS*–procedure ($\overline{M}_I^{RS}$) provide values which are lower than $\overline{M}_I^{std,asym}$ and closer to the observed ones. In fact, for NGC 1868, NGC 2209, and $Hodge\,14$ we find respectively $\overline{I}^{RS} = 16.6 \pm 0.5$, 16.4 ± 1.0, and 16.5 ± 0.9, which can be compared to the corresponding asymptotic values $\overline{I}^{std,asym} = 15.93 \pm 0.05$, 15.84 ± 0.05 and 16.06 ± 0.05. Note that similar computations performed for the massive cluster NGC 1866 give $\overline{I}^{RS} = 15.0 \pm 0.1$. SBF in the V–band show a similar behavior, in the sense that the agreement gets even better if $\overline{M}_V^{RS}$ values are compared to observations. Statistical effects are mainly driven by fluctuations in the number of giant stars, then for intermediate/old age populations they affect the I and NIR bands

more than the optical ones (Fig. 2).

Even with the present large error–bars and the limited sample of LMC clusters we are dealing with, we can reach the following conclusions:

1. SSP models including TP stars reproduce optical SBF of LMC clusters reasonably well. This rules out the extremely high mass–loss rate, thus driving stars to an early departure from the AGB;

2. A mild mass–loss rate (BH) appears inadequate, because too much TP stars are foreseen. SSPs predict a very 'red' $(\overline{V}-\overline{I})$ color, which is not supported by the observed SBF values.

3. $B1$– and $B2$–models seem to predict a number of TP stars which can reproduce the SBF of the selected sample of LMC clusters.

Due to the relatively small number of LMC clusters included in our sample, the previous conclusions must be regarded as important, though not conclusive, indications. Further observational efforts are requested, both in improving the size of the sample and in minimizing the uncertainties of the measurements.

5.2. NIR SBF

G04 recently provided *JHK* SBF–measurements of eight 'super–clusters' as obtained from 2MASS observations of several LMC and Small Magellanic Cloud (SMC) stellar clusters. Each super–cluster groups clusters within a given range of the s–parameter (Elson & Fall 1985), and corresponds to a SWB class (Searle et al. 1980). The SBF derived from these super-clusters have the remarkable advantage of relying upon a large number of bright stars. For this reason, we compared present models with those NIR data.

Differently from Gonzalez and collaborators, who used the Cohen (1982) ages for the SWB classes, we adopted the age calibration of the s–parameter from two more recent works: Elson & Fall (1988) and Girardi et al. (1995). They provide similar results (within $5-10\%$) even if one is based upon *canonical* stellar models ($log\ t = 6.05 + 0.079s$: Elson & Fall 1988) and the other one on *overshooting* stellar models ($log\ t = 6.227 + 0.0733s$: Girardi et al. 1995).

In Fig. 10 we plot our *JHK* SBF predictions as a function of age for different metallicities, and the $B1$–models. The observational data published by G04 (as corrected after Gonzalez et al. 2005) are reported as filled squares, with the related ages according to the

canonical calibration. The age error–bars refer to the ages corresponding to the initial and final s–parameter values of the clusters included in each super-cluster. We re–scaled G04 measurements to the LMC distance adopted in previous Sections. The models are calculated for slightly different K–band filter than 2MASS K–band filter (K_s), but the differences are negligible for our present purpose (Carpenter 2001).

The general behavior of *JHK* SBF data is reproduced by models in all NIR bands. Both models and data show a jump around $30 - 50\,Myr$ corresponding to the appearance of red and bright AGB stars. After that, the luminosity of the AGB–tip decreases with age, and the SBF NIR data decline accordingly. In spite of the qualitative agreement concerning the general trend, the quality of the fit is *not* satisfactory.

The comparison shows that SBF from $B1$–models are systematically fainter than NIR SBF magnitudes of the MC super–clusters. In the range from a few hundreds Myr to few Gyr, only super–solar SSP models give SBF magnitudes as bright as G04 data. It is well known that MC clusters have chemical abundances lower or at most equal to the solar value, so that metallicity variations do not appear to properly solve the quoted discrepancy. Other models (G04) also require unlikely high values of metallicity to reproduce the SBF measurements obtained for super–clusters.

We evaluated the impact of increasing the number of cool bright AGB stars by comparing the super–cluster data to the SBF predictions obtained by BH–models. Fig. 11 (left panel) shows that J–band SBF magnitudes seem to be well fitted by BH–models with reasonable metallicity values. Unfortunately, these models fail in reproducing K–band measurements, since the theoretical SBF amplitudes are brighter than the data for $t \sim 100 Myr$ and fainter for older ages (Fig. 11, right panel). Hence, this scenario seems to be ruled out, too.

Which kind of stars are missed in the models and what place should they occupy in the CMD in order to move the theoretical NIR SBF magnitudes to the observed values? Note that SBF predictions in the optical bandpasses should not be affected by including that kind of stars, because the SBF in that range of wavelength can fit observations. This leads to investigate the lack of cool bright stars in our models. In order to reproduce exactly the SBF of super–clusters, we performed numerical experiments by assembling the number of simulations needed to form a super–cluster with a total mass $\mathcal{M} \sim 4 \cdot 10^6\,M_\odot$, representing an average value from classes II to VII of G04 at a given age ($B1$–models and $Z = 0.008$). Obviously, the SBF derived for these theoretical super–clusters resemble – within the uncertainties – the SBF reported in Table 1, because we are dealing with asymptotic values.

As a first approximation, we verify what happens to theoretical NIR SBF if a contami-

nation of LMC supergiant M–type field stars is included (Nikolaev & Weinberg 2000). Fig. 3 by G04 shows that a non negligible number of bright stars at $K_s \simeq 10$ and $J - K_s \simeq 1$–1.2 are present in the super–clusters corresponding to I–IV SWB classes. If such a small contamination of field stars is included into our theoretical super–clusters, we find that models shift towards a higher luminosity. Furthermore, the presence of NIR–bright AGB stars displaying ^{12}C enrichment, due to the third dredge–up (C–stars), also affects SBF in these bands. The K_s *vs.* $J - K_s$ CMDs of the super–clusters (Fig. 3 of G04, SWB classes IV, V and VI) show stars with $J - K \gtrsim 1.3 - 1.4$, the typical value used to select C–stars photometrically in the SMC and LMC (Cioni et al. 2001; Cioni et al. 2003, Raimondo et al. 2005). Cohen (1982) already stated that these classes are "precisely those where integrated light (Persson et al. 1983) and searches among the brightest red stars (Frogel & Cohen 1982; Aaronson & Mould 1982) have revealed the presence of luminous carbon stars.". If this is the case, the discrepancy between NIR data and models should be reduced by moving from K– to J–band, and is expected to become negligible in the optical range. This is exactly what happens – as shown in Fig. 10(a, b, c). From Fig. 3 of G04, we note that SWB classes V and VI show a narrow giant branch with a group of stars redder than $J - K \gtrsim 1.4$, roughly 10 and 4 for SWB classes V and VI, respectively. By adding these stars to our theoretical super–clusters, SBF predictions go up to the same position of observational values (Fig. 12).

All in all, these numerical experiments lead to the conclusion that models with the proper MC metallicity can be reconciled with observed NIR SBF for MC super–clusters if: 1) a field contamination of M–type stars is assumed, *and* 2) the number of stars with $J - K \gtrsim 1.3 - 1.4$ is increased in the SSP models.

In spite of the fairly good agreement obtained in Fig. 12, we explored a further possibility. Let us recall that super–clusters are not really SSPs, being the results of a sum of individual stellar clusters with slightly different ages and chemical compositions. In addition, the membership of an individual cluster to a given SWB class may be uncertain (Girardi et al. 1995). Thus, we investigated the possibility that super–clusters contain a certain fraction of populations younger than the minimum age assigned to the corresponding SWB classes. This suggestion is supported by the fact that CMDs of I, II, III, and IV SWB classes in Fig. 3 by G04 exhibit features which could be related to the presence of populations with chemical compositions and/or ages different from the corresponding SWB class (see for example the bi–modal red giant branches).

Numerical experiments performed for SWB classes from II to VI show a relevant increment of the SBF magnitudes if a stellar population younger than the typical age value assigned to the corresponding SWB class is included. In particular, we find that the presence of one (or few) younger cluster leads to predict SBF in agreement with observations

(Fig. 13). Keeping in mind that the results in Fig. 13 do not represent the only solution, we note that the percentage of the young population required to predict the SBF NIR data is of the order of 10%. In other words, if one (or few) cluster is included in a given SWB class because of its s–parameter is overestimated (for whatever reason, see Girardi et al. 1995), this leads to brighten the SBF amplitudes for that SWB class. On the contrary, numerical experiments show that an underestimation of the s–parameter of one (or few) cluster would not significantly affect the super–cluster SBF measurements.

In conclusion, we showed that NIR SBF of the super–clusters by G04 can be reproduced – though not in a definitive way. Further observational and theoretical efforts are required to improve the understanding of NIR SBF amplitudes of young and intermediate age stellar populations.

6. Summary and Conclusions

We presented new theoretical SBF amplitudes for single–burst stellar populations of young and intermediate age ($25\,Myr \leq t \leq 5\,Gyr$) and metallicity ranging from $Z = 0.0003$ up to 0.04. The new SBF models are based on an updated version of the stellar population synthesis code already used to derive SBF for old stellar populations in Paper I. In the present version of the code, we used the recently published evolutionary–tracks database of Pietrinferni et al. (2004), and T_{eff}–colors relations from Westera et al. (2002). A particular care has been paid to the simulation of the properties of intermediate–mass AGB stars experiencing the TP–phase. The time evolution of core mass, and luminosity, together with the overall evolutionary time–scale of these stars have been evaluated according to prescriptions by WG98. Additionally, the number of TP–AGB stars is also triggered by mass–loss efficiency. Therefore, in order to evaluate the impact of this type of stars upon fluctuation amplitudes, three different mass–loss scenarios were simulated (BH, $B1$, and $B2$), along with the extreme case of no TP–stars at all.

The resulting new database of stellar population models covers a wide range of chemical compositions and ages. The accurate SSP models allowed us to successfully fit the observed CMD features of a sample of LMC star clusters imaged with the WFPC2/HST (V and I bands). Age, metallicity, and reddening for all clusters are derived and successfully compared with literature estimations.

Owing to the Monte Carlo technique, which is the basis of our method to derive fluctuation amplitudes, we estimated the cluster integrated magnitude M_V^{Tot} required to minimize indetermination caused by stochastic effects due to random variation of the number of bright

stars affecting SBF measurements. We find that the procedure used to compute SBF from individual stars of a synthetic CMD (RS–procedure) provides –within uncertainties– the same results as the *std*–procedure if $M_V^{Tot} \lesssim M_V^{Tot,max}$, being $M_V^{Tot,max}$ a function of the stellar population age and metallicity. This has a direct application in the observational field. Firstly, once the absolute integrated magnitude of the measured sample of stars is known, the RS–procedure provides a tool to evaluate the intrinsic uncertainty of SBF measurements as derived by individual stars photometry of a real stellar system (Fig. 2). Secondly, the SBF derived from the photometry of spatially resolved systems can be compared properly with the theoretical SBF asymptotic values only if the stellar system integrated magnitude satisfies the condition $M_V^{Tot} \lesssim M_V^{Tot,max}$, otherwise stochastic effects prevent a reliable and meaningful comparison.

By focusing the attention on optical SBF, we performed the first V and I bands SBF measurements for 11 LMC cluster by using the WFPC2/HST photometry of individual stars. The explored age ranges from $\sim 10\,Myr$, for the very young cluster NGC 1805, up to the typical age of Galactic globulars (NGC 1754, NGC 1916, NGC 2005, NGC 2019). The comparison of SBF measurements with our models showed a good agreement with both observed fluctuation magnitudes and colors if metallicities of $Z = 0.008$–0.01 and $Z = 0.001$–0.0001 are adopted respectively for young/intermediate age and very old clusters. The $(\overline{V}-\overline{I})$ fluctuation color has been found to be sensitive to the adopted mass–loss scenario along the TP–phase. The comparison between SBF models and measurements suggests that B95 mass–loss rates better simulate the observed LMC clusters fluctuation colors.

Few interesting features have been identified in the time–evolution behavior of fluctuation magnitudes and colors of the present models. Sizable variations arise at $t \sim 50\,Myr$ and $t \sim 1\,Gyr$. These jumps correlate with the RGB– and AGB–phase transitions. For stellar populations younger than $1\,Gyr$ the high sensitivity exhibited by SBF magnitudes to age variation supports the use of the SBF tool to evaluate ages of young stellar clusters in Local Group galaxies.

The capability of the stellar population synthesis code of directly managing parameters and physical processes characterizing the TP–AGB evolutionary phase allows us to analyze in depth the SBF dependence on TP–AGB stars. It is worth remarking that the different mass–loss scenarios affect both SBF magnitudes and colors for populations older than $1\,Gyr$ only for few tenths of magnitudes, confirming results given in Paper I. On the other side, for $t < 1\,Gyr$ the SBF amplitudes appear to be highly dependent on the adopted mass-loss scenario. Therefore, in this age range SBF can be used to infer information on the mass-loss efficiency of both resolved and unresolved young stellar populations.

The comparison with NIR SBF observations of MC super–clusters has shown that our

models reproduce the general trend of the data but a deeper analysis discloses that unlikely high values of metallicity are required to fit the super–clusters data. We have shown that composite stellar populations or contamination by field stars coupled with a more precise simulations of very cool stars (C–stars) may reconcile NIR SBF of MC super–clusters with theoretical predictions.

Therefore, SBF studies in both the optical and NIR regime evidence that further theoretical and observational efforts are needed to improve the models accuracy, and the reliability of measurements for nearby well known objects. On the other side, SBF should be regarded as a very valuable tool to improve our knowledge of unresolved stellar populations in distant galaxies for which SBF measurements can be used to detect the presence of young and intermediate age stellar populations, and to investigate their evolutionary properties more efficiently than "classical" integrated light studies.

We thank Dr. R. González-Lópezlira for providing constructive and insightful comments that have greatly improved the paper. It is a pleasure to acknowledge Adriano Pietrinferni and Santi Cassisi for providing evolutionary tracks, and S. Shore for useful discussions and for a careful reading of the manuscript. Financial support for this work was provided by MIUR–Cofin 2003. This work made use of computational resources granted by the Consorzio di Ricerca del Gran Sasso according to the Progetto 6 *'Calcolo Evoluto e sue Applicazioni (RSV6)'*–Cluster C11/B. This paper is based on observations made with the NASA/ESA Hubble Space Telescope, obtained from the ESO/ST-ECF Science Archive Facility, and data products from the Two Micron All Sky Survey, which is a joint project of the University of Massachusetts and the Infrared Processing and Analysis center/California Institute of Technology, funded by the National Aeronautics and Space Administration and the National Science Foundation.

A. Modelling the TP–AGB stellar evolution phase

The present SSP models rely on the evolutionary–tracks database by P04, which include all the most updated physical inputs in computing stellar models, as for example the new equation of state by Irwin et al. (2004), and recent nuclear reaction rates by Angulo et al. (1999), and Kunz et al. (2002) for the $^{12}C(\alpha,\gamma)^{16}O$ (see P04 for more details). The database covers a wide range of chemical compositions and stellar masses. Intermediate and low mass stellar models end up at the first thermal pulse, thus the evolution along the TP–AGB phase is not provided. Therefore, in the following we describe the procedure presently adopted to simulate this bright and fast evolutionary phase in our stellar population synthesis models

in order to properly compute SBF amplitudes.

Although it is well known that the AGB evolution of stellar masses $m \lesssim 6$–$8\,M_{\odot}$ (depending on metallicity) ends with a series of helium shell flashes or thermal pulses (TPs) (e.g. Iben & Renzini 1983), a series of difficulties in modelling these stars still arises. This depends from several physical mechanisms. Among others, we recall: 1) the treatment of convection, which is poorly known and commonly parameterized by the Mixing Length Theory (MLT) with the "mixing length scale" free parameter (usually indicated as α); 2) the mass–loss rate, for which observations indicate a value ranging from $10^{-7} M_{\odot}/yr$ to even $10^{-3} M_{\odot}/yr$ for the coolest and luminous red super–giants (Van Loon et al. 1999); 3) the occurrence of the Hot Bottom Burning (HBB), and of the third dredge–up, which regulate the formation of carbon–rich stars (C–stars); 4) the luminosity variations, which may reach an amplitude of the order of few magnitudes in V and few tenths in NIR bands (Cioni et al. 2001; Raimondo et al. 2005). Therefore, fully modelling the TP–AGB phase is indeed complex and time–consuming, thus stellar population models make use of 'analytic' approaches (WG98; Marigo 1998).

In intermediate and low mass stellar models by P04 the evolution is followed from the MS until the onset of TPs. To extend the track to the TP–phase we used the analytic formulas by WG98, simulating the behavior of each TP–AGB star, in terms of its core mass (m_c) and luminosity (L) as a function of time. The adopted relation between the maximum bolometric luminosity L during the quiescent hydrogen burning and the core mass m_c (in solar units) is:

$$\begin{aligned} L = \quad & (18160 + 3980z)(m_{\rm c} - 0.4468) + 10^{2.705\ +\ 1.649 m_{\rm c}} \times \\ & \times \left(10^{0.0237(\alpha - 1.447) m_{\rm c,0} 2 m_{\rm e} 2 (1 - {\rm e}^{-\Delta m_{\rm c}/0.01})}\right) - 10^{3.529\ (m_{\rm c,0} - 0.4468)\Delta m_{\rm c}/0.01} \end{aligned} \tag{A1}$$

where $z = log(Z/Z_{\odot})$ refers to the MS metal abundance, $m_{c,0}$ is the core mass at the first thermal pulse, Δm_c is defined as $\Delta m_c = m_c - m_{c,0}$, and m_e is the envelope mass. Concerning the MLT parameter, we assumed $\alpha = 2$ according to the value used by P04 in the previous evolutionary stages.

The equation of the core growth is:

$$\frac{{\rm d}m_c}{{\rm d}t} = \frac{q}{X_{\rm e}} L_{\rm H}, \tag{A2}$$

where q is the mass burnt per unit energy release, and $X_{\rm e}$ is the hydrogen in the envelope (mass fraction):

$$q = [(1.02 \pm 0.04) + 0.0017z] \times 10^{-11} (M_{\odot} L_{\odot}^{-1} yr^{-1}) \tag{A3}$$

$L_{\rm H}$ is the luminosity produced by H–burning, which is obtained by the following equation:

$$log\ (L_{\rm H}/L) = -0.012 - 10^{-1.25-113\Delta m_{\rm c}} - 0.0016 m_{\rm e}. \tag{A4}$$

Finally, the core mass–interpulse time relation is:

$$log\ \tau_{\rm ip} = (-3.628{+}0.1337z)(m_{\rm c}{-}1.9454){-}10^{-2.080\ 0.353z+0.200(m_{\rm e}+\alpha-1.5)}{-}10^{-0.626\ 70.30(m_{\rm c,0}-z)\Delta m_{\rm c}} \tag{A5}$$

We performed an integration of the system of equations obtaining, for each thermal pulse, the luminosity, the core mass, and the duration of the pulse. We also included a mass–loss rate regulating the total mass at each TP star, as extensively discussed in the next section. The stellar temperature is derived by using prescription of Renzini & Voli (1981), considering the appropriate slope d $log(L/L_{\odot})$ /d $log(T_e)$ for the evolutionary tracks we are using. The procedure ends by providing the 'expected' evolution of a star of a given mass during the TP–phase.

A.1. Mass–loss efficiency for TP–AGB Stars

In this work, mass loss is parameterized by following the prescription by Reimers (1975) along the RGB and on AGB until the first thermal pulse:

$$\dot{m}_R = -4 \cdot 10^{-13} \eta_R \cdot LR/m \tag{A6}$$

where L, R, m are respectively the star luminosity, radius and total mass in solar units; along these phases we assumed $\eta_R = 0.4$.

The quantitative determination of mass–loss rate along the TP–phase is a complex problem, since dust formation and circumstellar dust shells avoid in several case the possibility to observe stars in the optical band. Nevertheless, the duration of the TP–phase is triggered by the efficiency of the mass loss, thus to parameterize mass–loss processes we followed several prescriptions. After the first thermal pulse, we first used the formulation by BH, derived from statistical properties of OH/IR stars:

$$\dot{m}_{BH} = \mu LR/m_{\rm e} \tag{A7}$$

with $\mu = -4 \cdot 10^{-13}(m_{e,0}/m)$, being $m_{e,0}$ the envelope mass at the first TP. This is a modification of the Reimers formula with $\eta_R = 1$ which also includes a dependence on the actual mass envelope.

For the sake of clearness, the present TP evolution is compared with the results by other authors. In Table A.1 we report the TP evolution of a star with an original MS–mass $m_{MS} = 7\,M_{\odot}$, and solar metallicity with similar calculations by Marigo (1998, M98), and Blocker & Schoenberner (1991, BS91). Table A.1 lists thermal pulse number (Col. 1), mass of the star (Col. 2), core mass (Col. 3), and the star luminosity after a certain number of thermal pulses (Col. 4). The first block refers to the TP evolution obtained by adopting the procedure described above, starting from values of luminosity, temperature, and core mass at the first TP according to P04 (case *a*). The second block refers to the same TP procedure, but the initial values of luminosity, temperature, and core mass at the first TP are from BS91 (case *b*). The last two blocks report TP evolution by BS91 and M98. There is a fair agreement (within $\sim 10\%$ in luminosity) between block #2, and blocks #3 and #4. Larger differences are found if we make use of the stellar models by P04 (case *a*). This case foresees stars experiencing the TP stage at a level brighter than that found by M98 and BS91 (for example $\sim 25\%$ at TP #30). Note that, for the given mass ($m_{MS} = 7\,M_{\odot}$) tracks by P04 predict a higher luminosity at the first TP than those adopted by M98 and BS91.

As shown by B95, the BH formulation cannot well reproduce the observed initial–final mass relationship. He proposed a mass–loss rate based on dynamical theoretical investigation on the atmospheres of Mira–like variables by Bowen (1988). B95 suggested two mass–loss rates directly correlated with the stellar luminosity:

$$\dot{m}_{B1} = 4.83 \cdot 10^{-9} m_{MS}^{-2.1} L^{2.7} \dot{m}_R \tag{A8}$$

$$\dot{m}_{B2} = 4.83 \cdot 10^{-9} m_{TP}^{-2.1} L^{2.7} \dot{m}_R \tag{A9}$$

with $\eta_R = 1$. These formulas are valid for long period variable stars with periods $P > 100$ d. They differ in the adopted stellar mass: the case B1 makes use of the MS mass (m_{MS}), while B2 uses the actual mass (m_{TP}) predicting a steeper increase of the mass–loss rate. As an example, in the range of stellar masses we are interested in, the foreseen mass–loss rates in the case of $m_{MS} = 5M_{\odot}$, $Z = 0.02$, at the luminosity level $L \simeq 19600\ L_{\odot}$ are: $\dot{m} \simeq 6 \times 10^{-6}\ M_{\odot}/yr$ in the BH case; $\dot{m} \simeq 4.4 \times 10^{-5}\ M_{\odot}/yr$ for B1; and $\dot{m} \simeq 8.5 \times 10^{-5}\ M_{\odot}/yr$ in the B2 case. The B95 scenarios foresee more efficient mass–loss rates than BH, predicting a lower number of stars and a shorter life–time along the TP–phase. The high sensitivity of SBF to mass–loss is shown Section 3.2, where we suggest that SBF might be used as calibrator of mass–loss rate also for young and intermediate stellar populations, similarly to

old stellar systems (Paper I).

B. About the stochastic effects on SBF measurements

In order to deepen the matter of stochastic effects due to variations of the number of bright stars, we performed numerical experiments by varying the stellar population total mass $\mathcal{M}$. Fig. 14(a, c, e) illustrates how I–SBF amplitude is affected by stochastic effects depending on the star cluster richness, as a function of N_{sim}. Solid (red) lines refer to SBF derived by using the *std*–procedure based on integrated fluxes [Eq. 1: $\overline{M}_I^{std}(N_{sim})$]; dots represent SBF derived from the RS–procedure to the $j-$th simulation (Eq. 4: $\overline{M}_I^{RS,j}$). We consider SSPs with $t = 100\,Myr$ and $Z = 0.008$. The total mass increases from the top to the bottom.

First of all, we focus the attention on $\overline{M}_I^{RS,j}$. For small values of the SSP mass, stars belong typically to the MS, as indicated by the corresponding CMD (Fig. 14b). Due to the small number of stars, only a few simulations have few occasional stars burning He in the core, and even less simulations have the odd AGB stars. Correspondingly, $\overline{M}_I^{RS,j}$ is dominated by MS stars (Fig. 14a, the bulk of dots at $M_I^{RS,j} \sim -1\,mag$). When few He–burning stars appear in the CMD, the I–SBF becomes brighter ($\overline{M}_I^{RS,j} \sim -3\,mag$), and even brighter if a TP–AGB star appears in the simulation ($\overline{M}_I^{RS,j} \sim -6.5\,mag$, the few five–pointed stars).

By increasing the stellar population mass, the number of He–burning stars and AGB stars grows in the CMD: first the He–burning phase (Heb) becomes well populated (Fig. 14d), then for a further increase of the total mass a large number of stars populates the AGB and TP–AGB phases (Fig. 14f). Correspondingly, the SBF signal is always dominated by those evolved stars (Fig. 14c, e). Therefore, the scatter of the SBF signal inversely correlates with the stellar population mass $\mathcal{M}$: $\overline{M}_I^{RS,j}$ brighter than $-5\,mag$ are never produced by SSPs with $\mathcal{M} = 2.5 \cdot 10^5\,M_\odot$ while a few simulations among SSPs with $\mathcal{M} = 5 \cdot 10^2\,M_\odot$ can reach $\overline{M}_I \sim -6.5\,mag$. The reason is that for lower $\mathcal{M}$ the fluctuation for the few simulations with bright stars is larger than the fluctuation of the typical simulation without bright stars.

Red solid lines in Fig. 14 (left panels) illustrate how the SBF signal derived using the *std*–procedure becomes stable with N_{sim} approaching the *asymptotic value*. Discontinuities in the solid lines are directly related to the appearance of one or more very bright stars in the simulation (e.g. Fig. 14a). By increasing the total mass of the population, this event occurs with a higher probability, and discontinuities tend to disappear. If we add stars to the population, we obtain a *faster* convergence of $\overline{M}_I^{RS,j}$ to the *asymptotic value* $\overline{M}_I^{std,asym}$ (Fig. 14c, e).

Before closing this Appendix, let us make a further consideration on Fig. 14. From the figure, one can note that $\overline{M}_I^{std}$ tends to converge rapidly to the *asymptotic value* already after $N_{sim} \sim 500$ simulations when $\mathcal{M}_{tot} \geq 5 \cdot 10^3\, M_\odot$. However, even in the case of very poorly populated clusters (Fig. 14*a*) this happens before 2000 simulations. This feature has an important implication on the SBF measurements of unresolved populations in distant galaxies. In fact, the *standard* procedure approaches the observational way of deriving SBF in the case of unresolved stellar populations. In such cases, the integrated flux we compute for each j–th simulation corresponds to the flux measured in a single pixel of a distant galaxy image (if one neglects seeing and population mixture). Within the limit of this approximation, we find that after cleaning processes (masking, galaxy subtraction, etc.) the effective number of pixels used in deriving SBF measurements from a galaxy CCD image should be larger than 2000, searching for the presence of a young stellar population with a mass density lower than $10^3\, M_\odot$/pixel. In case of higher density (say $\gtrsim 10^4\, M_\odot$/pixel), the constraint becomes less severe and 500 pixels are enough to measure SBF with an uncertainty lower than $0.1\, mag$.

REFERENCES

Alcock, C., Alves, D. R., Axelrod, T. S., Becker, A. C., Bennett, D. P., Clement, C. M., Cook, K. H., Drake, A. J., Freeman, K. C., et al. 2004, AJ, 127, 334

Aaronson, M., & Mould, J. 1982, ApJSS, 48, 161

Ajhar, E. A., & Tonry, J. L. 1994, ApJ, 429, 557 (AT94)

Angulo, C., Arnould, M., Rayet, M., et al. 1999 (NACRE collaboration) Nucl. Phys. A, 656, 3

Baud, B., & Habing, H. J. 1983, A&A, 127, 73 (BH)

Blakeslee, J. P., Vazdekis, A., Ajhar, E. A. 2001, MNRAS, 320, 193

Blocker, T., & Schoenberner, D. 1991, A&A, 244, L43 (BS1)

Blocker, T. 1995, A&A, 297, 727 (B95)

Bowen , G.H. 1988, ApJ, 329, 299

Brocato, E., Capaccioli, M., Condelli, M. 1998, Mem. SAIt, Vol. 69, p.155

Brocato, E., Castellani, V., Di Carlo, E., Raimondo, G., Walker, A. R. 2003, AJ, 125, 3111

Brocato, E., Castellani, V., Poli, F.M., & Raimondo, G. 2000, A&AS, 146, 91

Brocato, E., Castellani, V., Raimondo, & G., Romaniello M. 1999, A&AS, 136, 65

Buzzoni, A. 1993, A&A, 275, 433

Cantiello, M., Raimondo, G., Brocato, E., & Capaccioli, M. 2003, AJ, 125, 2783 (Paper I)

Cantiello, M., Blakeslee, J. P., Raimondo, G., Mei, S., Brocato, E., Capaccioli, M. 2005, ApJ in press, astro-ph

Carpenter, J. M. 2001, AJ, 121, 2851

Castellani, V., Degl'Innocenti, S., Marconi, M., Prada Moroni, P. G., Sestito, P. 2003, A&A, 404, 645

Cioni, M.-R. L., Blommaert, J. A. D. L., Groenewegen, M. A. T., Habing, H. J., Hron, J., Kerschbaum, F., Loup, C., Omont, A., van Loon, J. Th., Whitelock, P. A., Zijlstra, A. A 2003, A&A, 406, 51

Cioni, M.-R. L., Marquette, J.-B., Loup, C., Azzopardi, M., Habing, H. J., Lasserre, T., Lesquoy, E. 2001, A&A, 377, 945

Cohen J. G. 1982 ApJ, 258, 143

de Grijs, R., Johnson, R. A., Gilmore, G. F., Frayn, C. M. 2002a, MNRAS, 331, 228

de Grijs, R., Gilmore, G. F., Johnson, R. A., Mackey, A. D. 2002b, MNRAS ,331, 245

de Grijs, R., Gilmore, G. F., Mackey, A. D., Wilkinson, M. I., Beaulieu, S. F., Johnson, R. A., Santiago, B. X. 2002c, MNRAS, 337, 597

Dolphin, A. E. 2000a, PASP, 112, 1383

Dolphin, A. E. 2000b, PASP, 112, 1397

Elson, R. A. W. & Fall S. M. 1985, ApJ, 299, 211

Elson, R. A. W. & Fall S. M. 1988, AJ, 96, 1383

Frogel J. A., Cohen J. G. 1982, ApJ, 253, 580

Girardi, L., Chiosi, C., Bertelli, G., Bressan, A. 1995, A&A, 298, 87

Girardi, L., Bressan, A., Bertelli, G., Chiosi, C. 2000, A&AS 141, 371

Gonzalez, R. A., Liu, M. C., Bruzual, G. A., 2003, poster paper in Stellar Populations 2003, Conf. Garching, Germany, Oct. 6–10, 2003

Gonzalez, R. A., Liu, M. C., Bruzual, G. A. 2004, ApJ, 611, 27 (G04)

Gonzalez, R. A., Liu, M. C., Bruzual, G. A. 2005, ApJ, 621, 557

Groenewegen, M. A. T., Smith, C. H., Wood, P. R., Omont, A., Fujiyoshi, T. 1995, ApJ, 449, L119

Herwig, F., Blocker, T., Schoenberner, D., El Eid, M. 1997, A&A, 324, L81

Kunz, R., Fey, M., Jaeger, M., Mayer, A., Hammer, J. W., Staudt, G., Harissopulos, S., Paradellis, T. 2002, ApJ, 567, 643

Iben, I., Jr., & Renzini, A. 1983, ARA&A, 21, 271

Irwin A. W., et al. 2004 in preparation

Jensen J.B., Tonry, J.L., Barris, B.J., Thompson, R.I., Liu, M.C., Rieke, M.J., Ajhar, E.A., Blakeslee, J.P., 2003, ApJ, 583, 712

Lejeune, T., Cuisinier, F., & Buser, R. 1997, A&AS, 125, 229

Liu, M.C., Charlot, S., & Graham, J.R. 2000, ApJ, 543, 644

Liu, M.C., Graham, J.R., & Charlot S. 2002, ApJ, 564, 216

Mackey, A. D., & Gilmore, G. F. 2003, MNRAS, 338, 85 (MG03)

Marigo, P. 1998, A&A, 340, 463 (M98)

Marigo, P., Girardi, L., Chiosi, C. 2003, A&A, 403, 225

Mei, S., Quinn, P. J., & Silva, D. R. 2001, A&A, 371, 979

Nikolaev, S., & Weinberg, M. D. 2000, ApJ, 542, 804

Olsen, K. A. G., Hodge, P. W., Mateo, M., Olszewski, E. W., Schommer, R. A., Suntzeff, N. B., Walker, A. R. 1998, MNRAS, 300, 665

Pahre, M. A., Mould, J. R., Dressler, A. Holtzman, J. A., Watson, A. M., Gallagher, J. S., III; Ballester, G. E., Burrows, C. J., et al. 1999, ApJ, 515, 79

Pagel, B. E. J., & Edmunds, M. G. 1981, ARA&A, 19, 77

Persson, S. E., Aaronson, M., Cohen, J. G., Frogel, J. A., Matthews, K., 1983, ApJ, 266, 105

Pietrinferni, A., Cassisi, S., Salaris, M., Castelli, F. 2004, ApJ, 612, 168 (P04)

Pols, O. R., & Tout, C. A. 2001, MmSAI, 72, 299

Raimondo, G., Brocato, E., Cantiello, M., & Capaccioli, M. 2003, poster paper in Stellar Populations 2003, Conf. Garching, Germany, Oct. 6–10, 2003

Raimondo, G., Cantiello, M., Brocato, E., Capaccioli, M. 2004, MmSAIt, 75, 198

Raimondo, G., Cioni, M. R. L., Rejkuba, M., & Silva, D. R. 2005, A&A in press, astro-ph 0503561

Reimers, D. 1975, in Problems in stellar atmospheres and envelopes, New York, Springer-Verlag, p. 229–256.

Renzini, A., & Buzzoni, A. 1986, in Proceedings of the Fourth Workshop, Erice, Italy, March 12-22, 1985, Spectral evolution of galaxies (Dordrecht, D. Reidel Publishing Co.),195

Renzini, A. & Voli, M. 1981, A&A, 94, 175

Salaris, M., Percival, S., Brocato, E., Raimondo, G., & Walker, A. R. 2003, ApJ, 588, 801

Santos, J. F. C. Jr., & Frogel, J. A. 1997, ApJ, 479, 764

Scalo, J.M. 1998, The Stellar Initial Mass Function (38th Herstmonceux Conference) ed. by G. Gilmore and D. Howell, ASP Conf. Ser., Vol. 142, 1998, p.201

Searle L., Wilkinson A., Bagnuolo W. G. 1980 ApJ, 239, 803

Sodemann, M., & Thomsen, B. 1995, AJ, 110, 179

Stephens, A.W., Frogel, J.A., Freedman, W., Gallart, C., Jablonka, P., Ortolani, S., Renzini, A., Rich, R.M., Davies, R.M. 2001, AJ, 121, 2584

Straniero, O., Chieffi, A., Limongi, M., Busso, M., Gallino, R., Arlandini, C. 1997, ApJ, 478, 332

Tonry, J.L., Dressler, A., Blakeslee, J.P., Ajhar, E. A., Fletcher, A. B., Luppino, G.A., Metzger, M.R., & Moore, C. B. 2001, ApJ, 546, 681

Tonry, J.L., & Schneider D.P. 1988, AJ, 96, 807

van den Bergh, S. 1981, A&AS, 46, 79

Van Loon, J. Th., Groenewegen, M. A. T., de Koter, A., Trams, N. R., Waters, L. B. F. M., Zijlstra, A. A., Whitelock, P. A., Loup, C. 1999, A&A, 351, 559

Wagenhuber, J., & Groenewegen, M. A. T. 1998, A&A, 340, 183 (WG98)

Walker, A. R., Raimondo, G., Di Carlo, E., Brocato, E., Castellani, V., & Hill, V. 2001, ApJ, 560, L139

Westera, P., Lejeune, T., Buser, R., Cuisinier, F., & Bruzula, G. 2002, A&A, 381, 524

Westerlund, B. E. 1997: *The Magellanic Clouds*, Cambridge University Press

Westerlund, B. E., Azzopardi, M., Rebeirot, E., Breysacher, J. 1991, A&AS, 91, 425

Worthey, G. 1993, ApJ, 415, 91

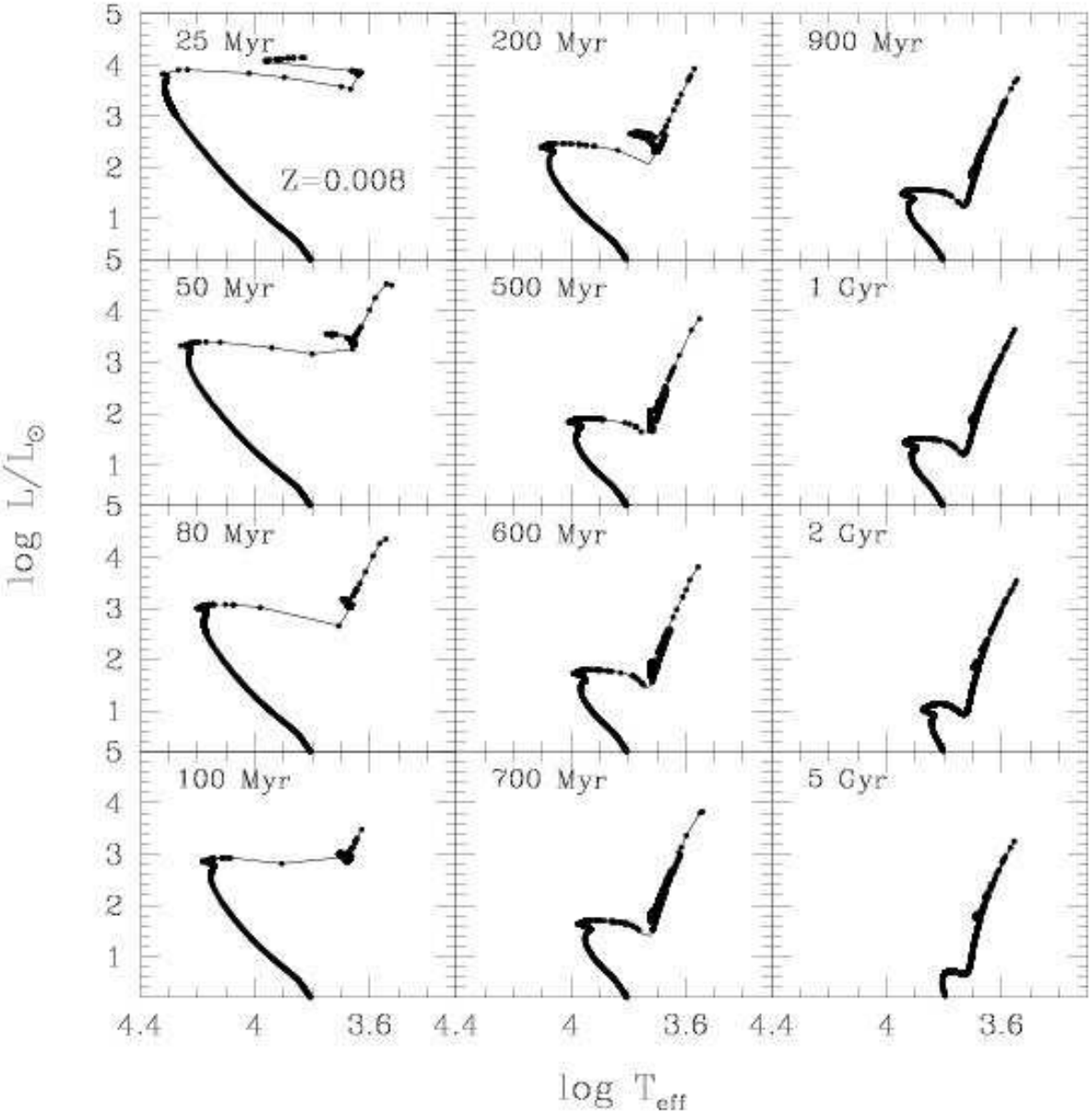

Fig. 1.— A sample of synthetic *log* $L/L_{\odot}$ *vs. log* T_{eff} diagrams for the labelled ages and $Z = 0.008$. In each panel one of the 5000 synthetic CMDs used to compute the SBF is plotted (dots); the line represents the isochrone. $B1$ mass–loss rate is assumed (see text and Appendix A).

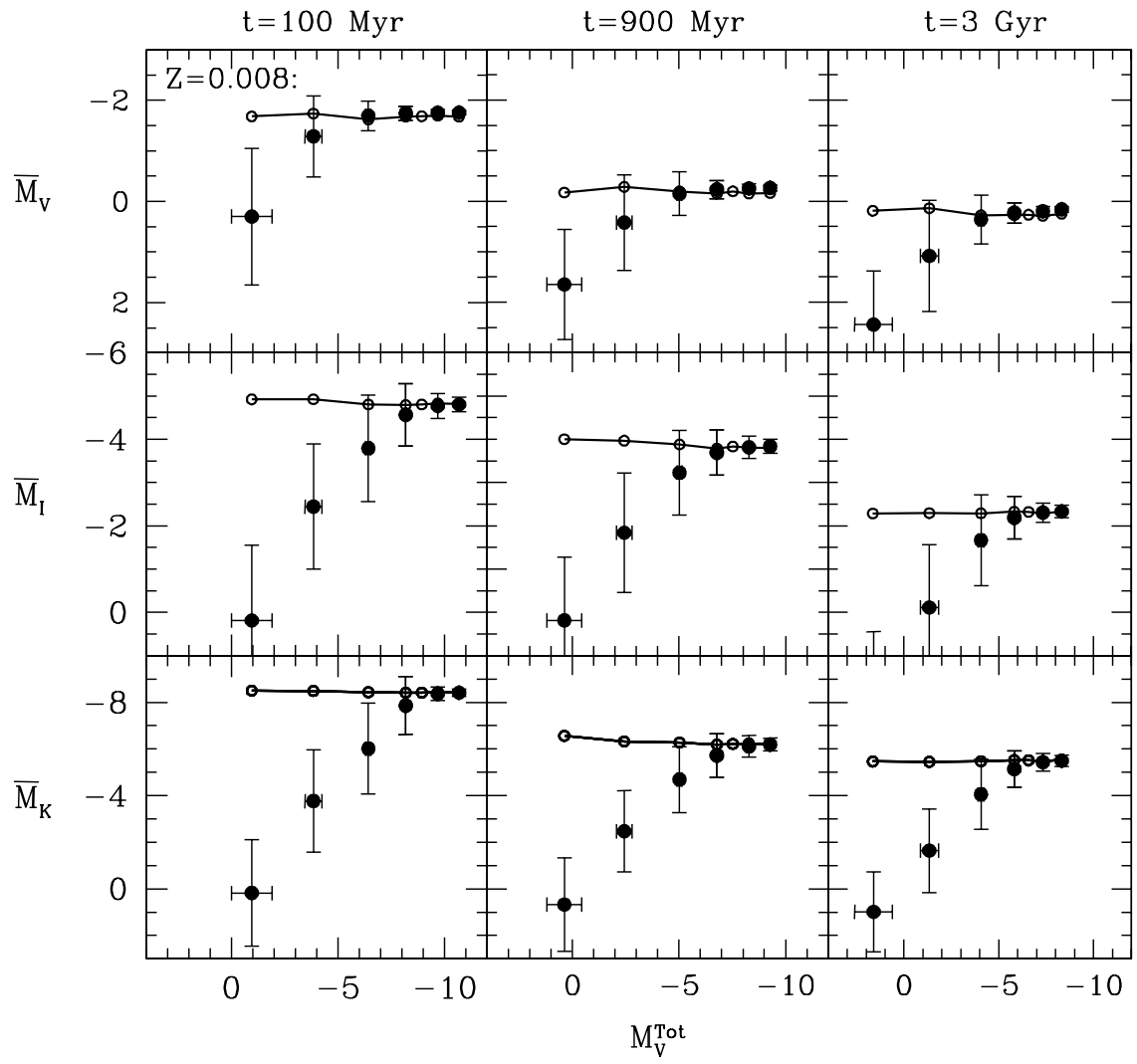

Fig. 2.— SBF absolute magnitudes as a function of the integrated absolute magnitude M_V^{Tot}. The thick solid lines (open circles) represent the *asymptotic SBF* ($\overline{M}_X^{std,asym}$, Eq. 1). Filled circles represent $\overline{M}_X^{RS}$ obtained from Eq. 5 (see text). Adopted metallicity and ages are labelled.

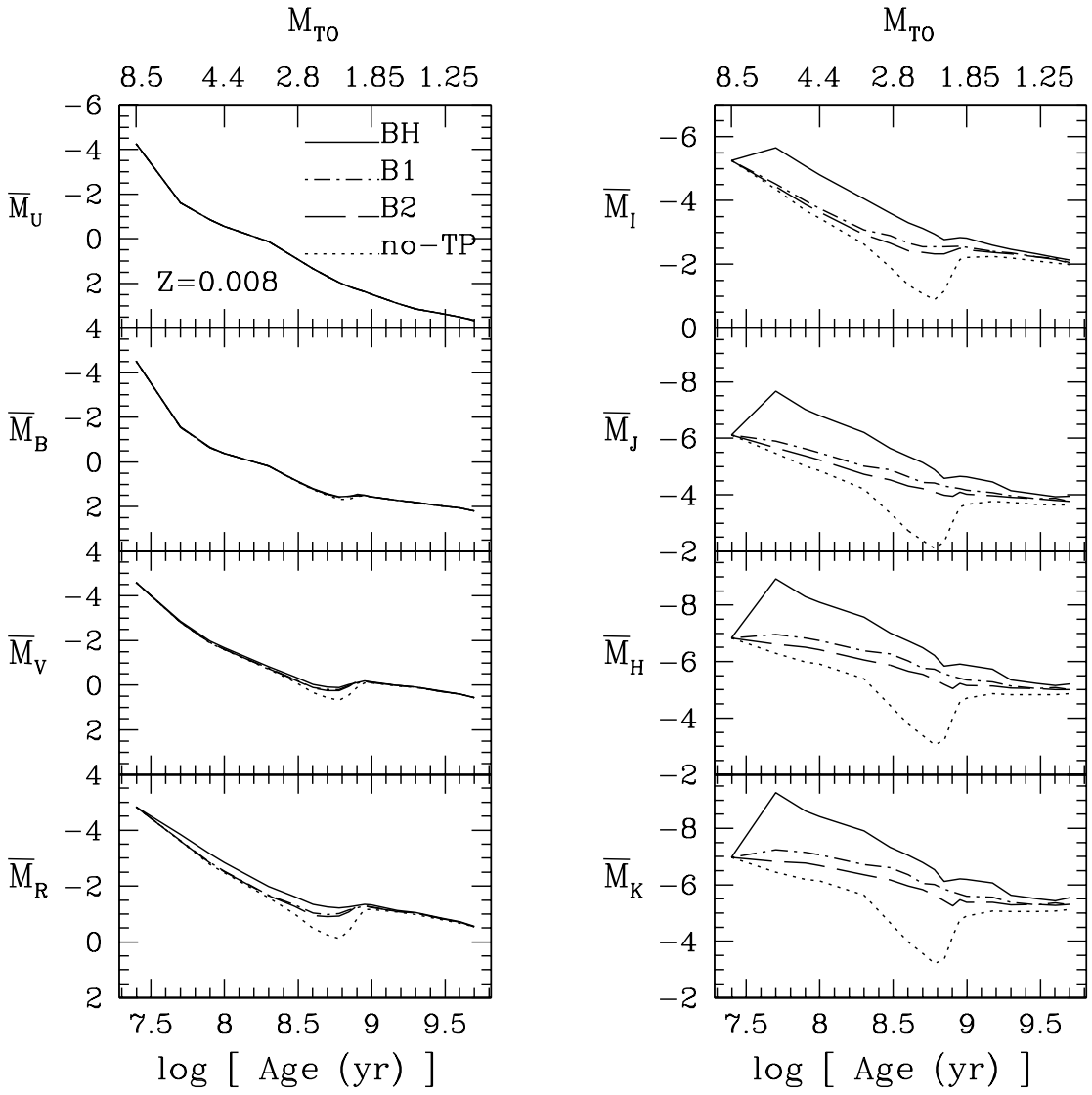

Fig. 3.— SBF magnitudes as a function of age, and fixed metallicity ($Z = 0.008$). Dotted lines correspond to models computed neglecting the TP–AGB phase (*no–TP*). Models including TP stars are plotted for three different mass–loss rate assumptions: *BH*–models (solid lines), *B*1–models (dot–dashed lines), and *B*2–models (long–dashed lines). The MS turn–off masses at selected ages are also labelled.

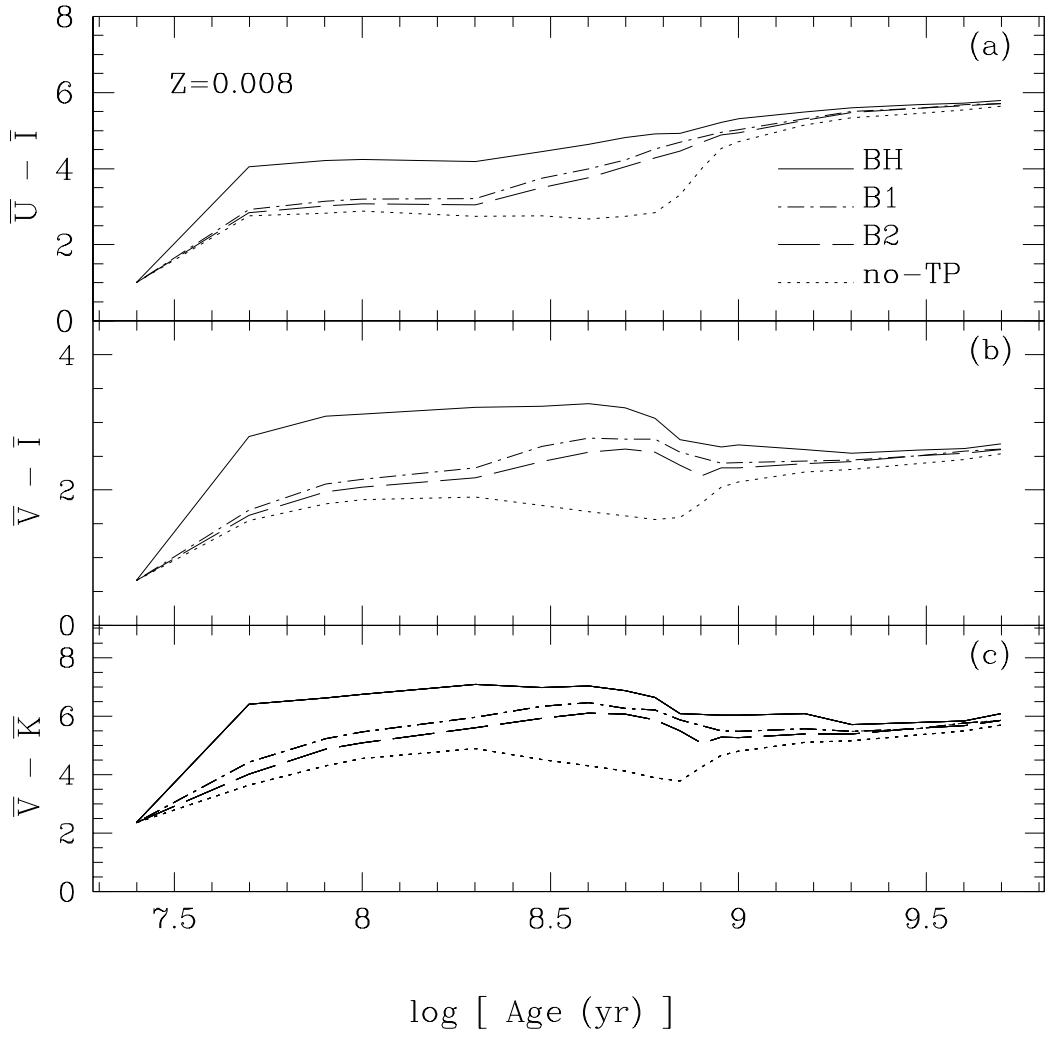

Fig. 4.— $\overline{U} - \overline{I}$, $\overline{V} - \overline{I}$, and $\overline{V} - \overline{K}$ fluctuation colors as a function of age, and fixed metallicity ($Z = 0.008$). Symbols are as in Fig. 3. The sensitivity to mass–loss rate assumed in modelling the TP–AGB phase is evident in the plotted colors.

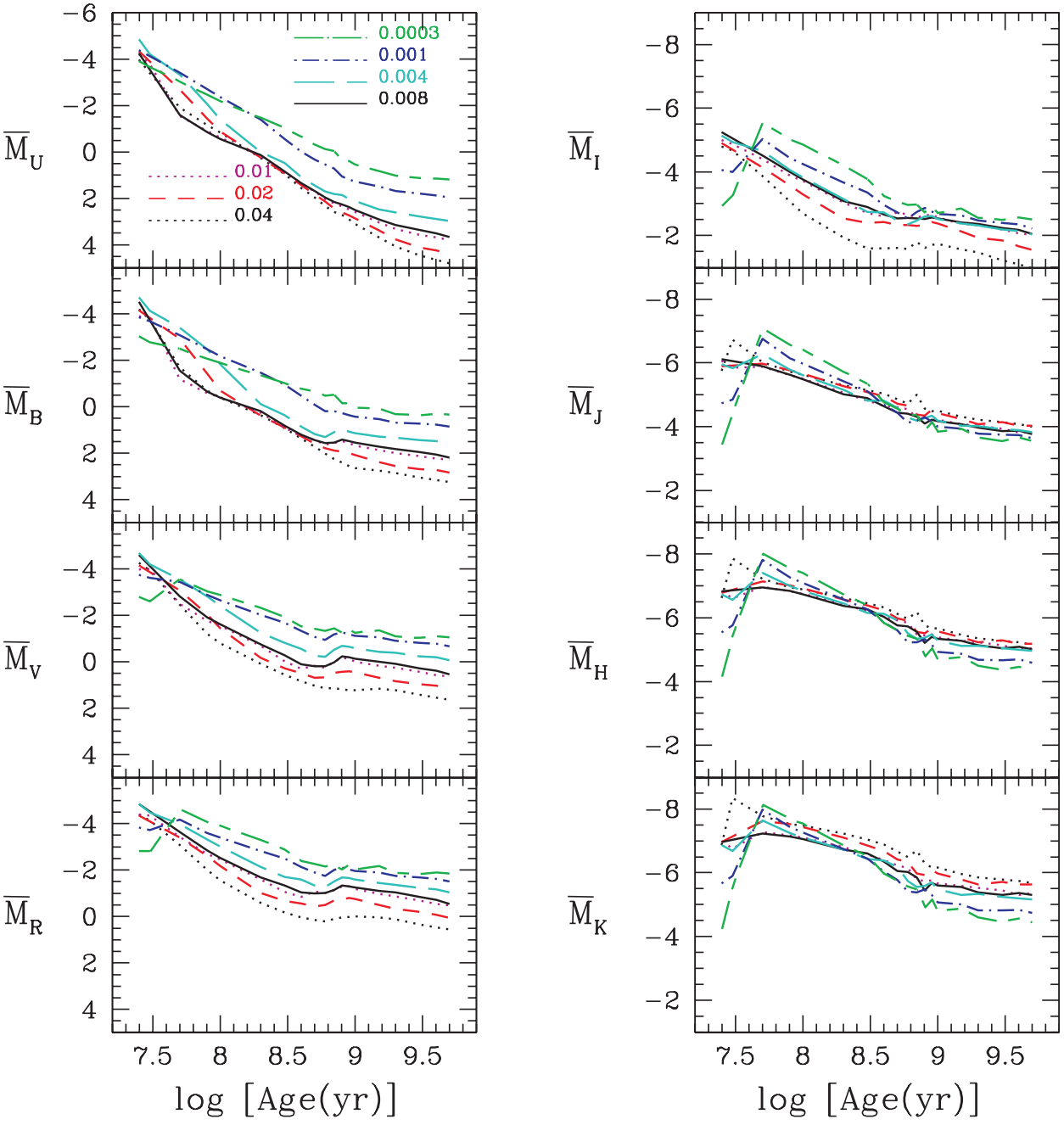

Fig. 5.— Time evolution of SBF magnitudes for different metallicities ($B1$–models). The different lines represent the labelled metallicity values.

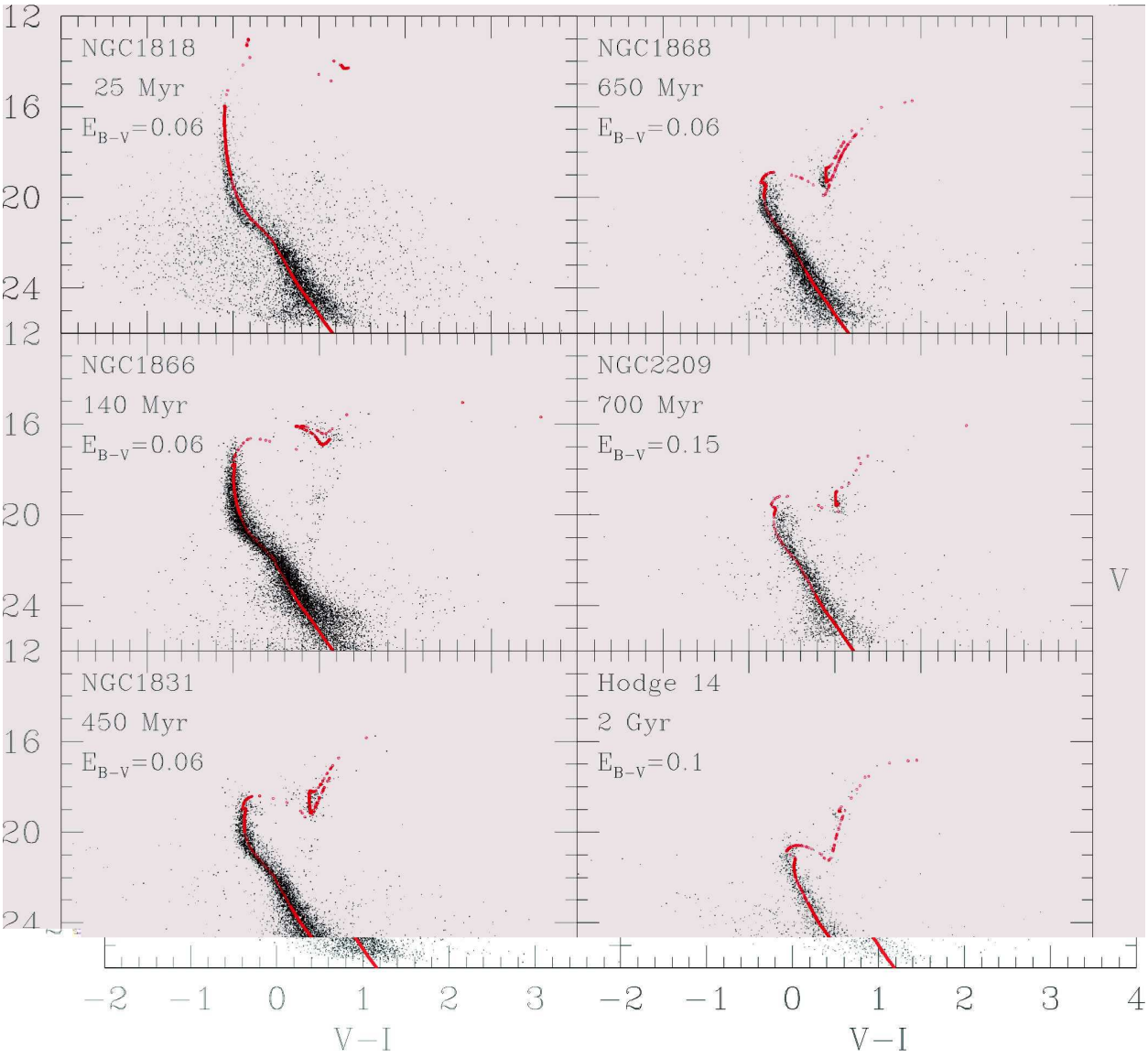

Fig. 6.— Observed (black dots) and synthetic (red dots) CMDs of a sample of LMC clusters are compared. In each panel the best fit is plotted, together with the derived reddening value. $Z = 0.008$ and an absolute distance modulus of $(m - M_V)_0 = 18.4$ are adopted. Photometric errors are also indicated on the right side of each panel

.

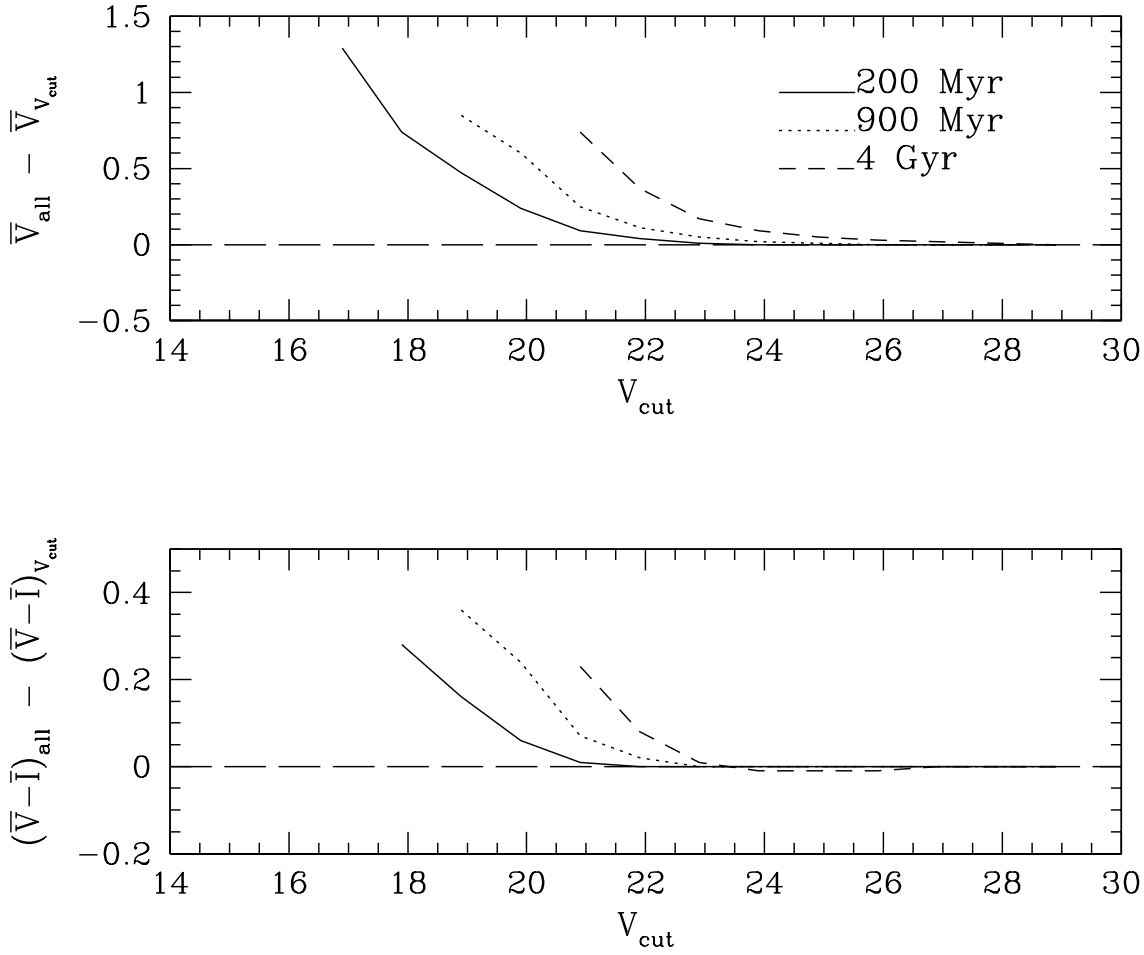

Fig. 7.— Impact of the completeness limit V_{cut} on SBF. The differences between SBF obtained using a synthetic CMD complete down to star mass $m = 0.1\,M_{\odot}$ and SBF from the same CMD but excluding stars with $V > V_{cut}$ (i.e. 100% of incompleteness at $V > V_{cut}$). The labelled ages and fixed metallicity $Z = 0.008$ are adopted.

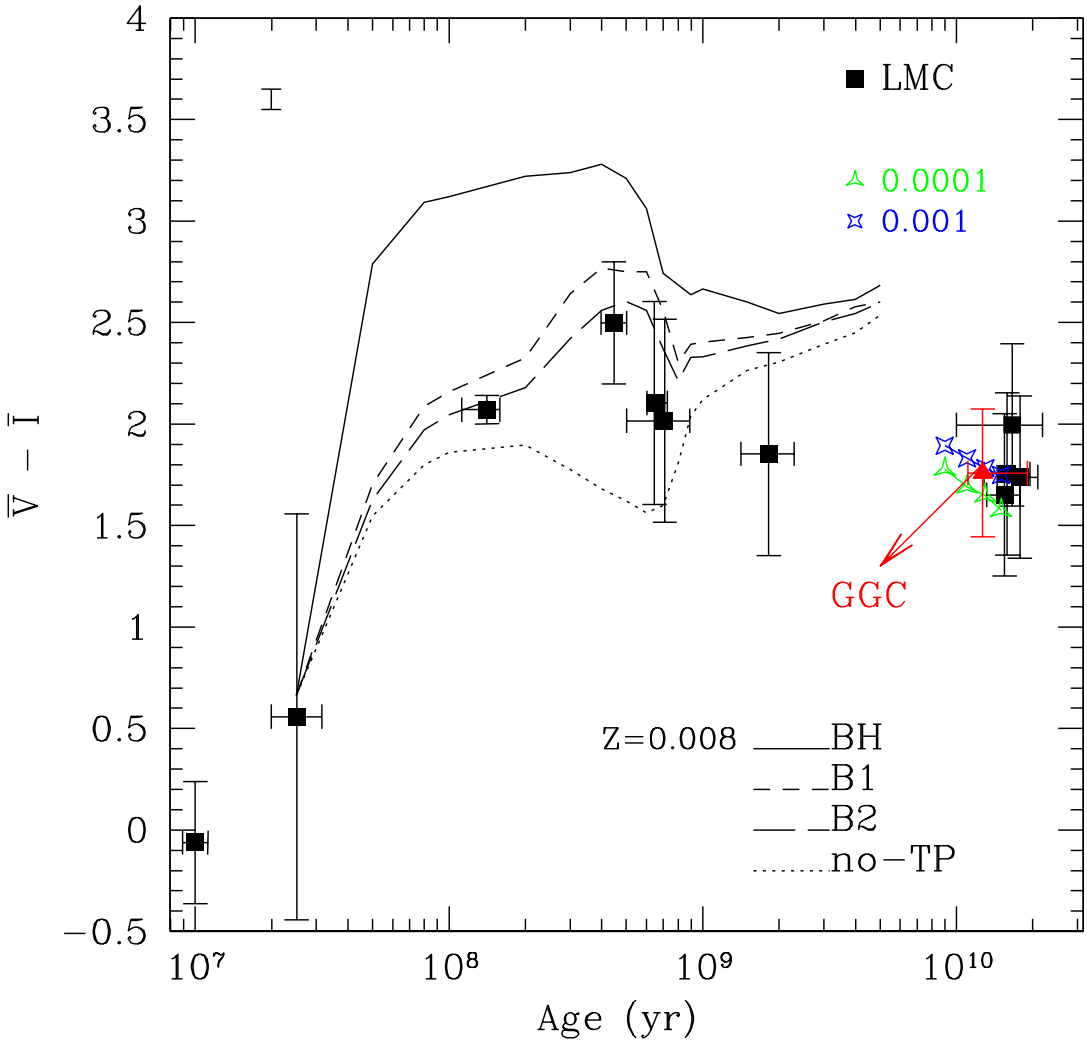

Fig. 8.— The $(\overline{V} - \overline{I})$ fluctuation color vs. age. For ages lower than $5\,Gyr$ models with $Z = 0.008$, and different mass–loss rates are plotted (symbols are as in Fig. 3). For ages larger than $5\,Gyr$ models with $Z = 0.0001$ (green three–pointed stars), and $Z = 0.001$ (blue four–pointed stars) are from Paper I. The LMC star clusters fluctuation colors are shown as black filled squares. The red triangle refers to the mean $(\overline{V} - \overline{I})$ color of GGCs (data from AT94). At the top left side we report the mean error–bar of SBF models.

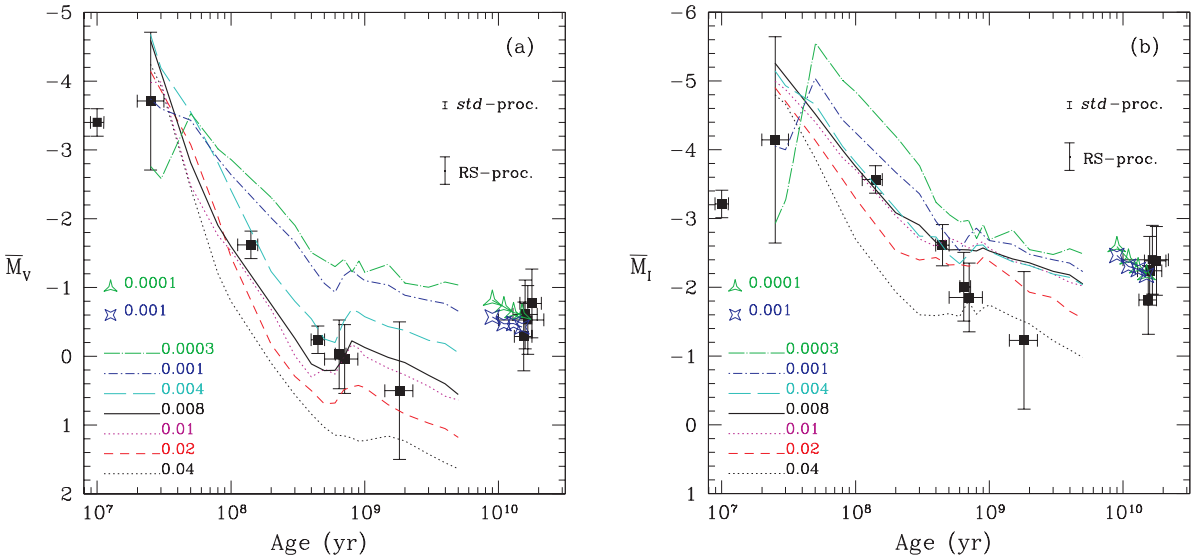

Fig. 9.— $\overline{M}_V$ (panel *a*) and $\overline{M}_I$ (panel *b*) are plotted as a function of age. For ages lower than $5\,Gyr$ models including $B1$ mass–loss rate are considered only. Models for $t > 5\,Gyr$ are from Paper I (symbols as in Fig. 8). Black filled squares refer to the measured SBF amplitudes for LMC star clusters. The expected theoretical uncertainties are shown at the upper right corner of each panel (see text).

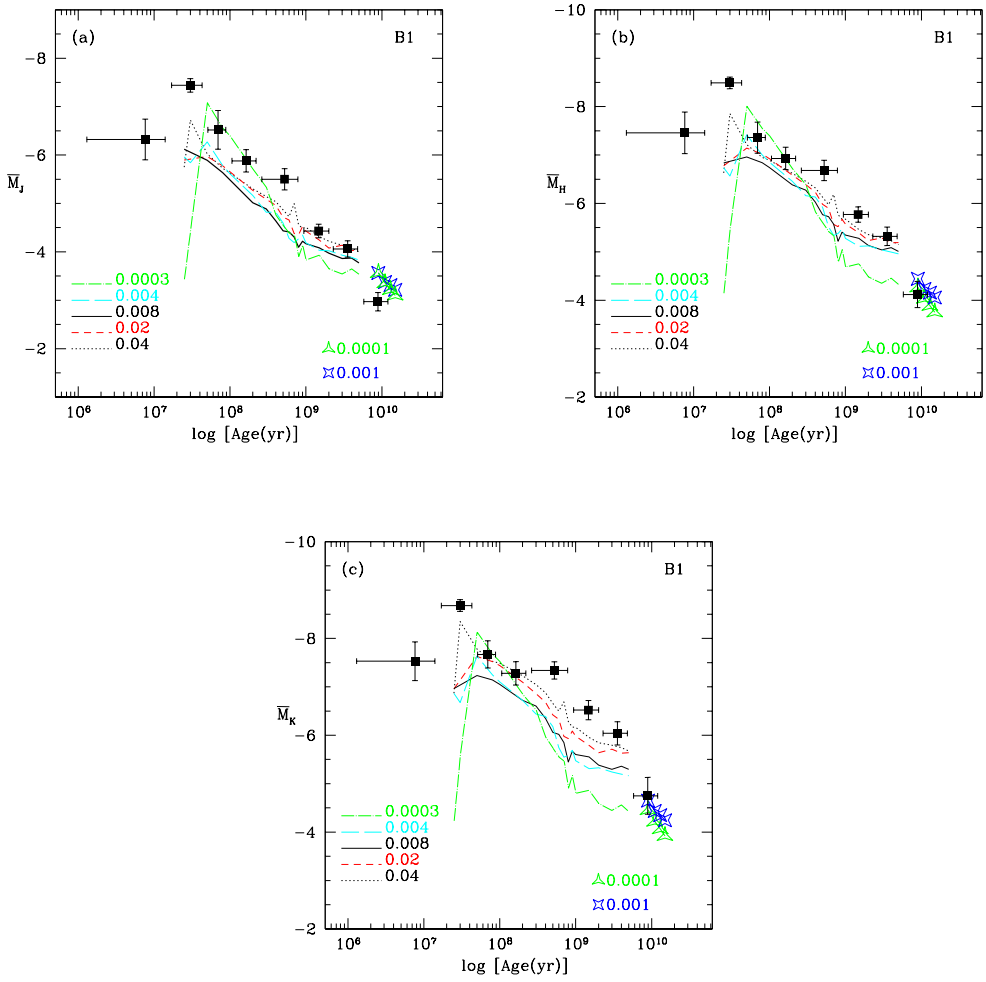

Fig. 10.— JHK SBF predictions of $B1$–models for selected values of metallicity as a function of age. Models for $t > 5\,Gyr$ are from Paper I (symbols as in Fig. 8). The SBF of MC super–clusters by G04 are plotted as filled squares. Age uncertainties cover the interval spanned by each SWB class according to the s–parameter values included in the super–clusters.

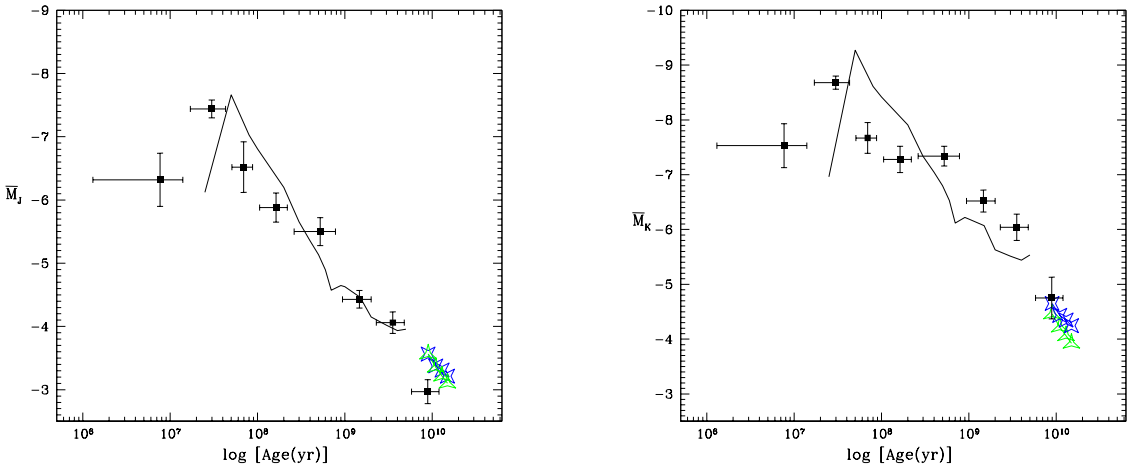

Fig. 11.— J– and K– SBF predictions obtained by BH–models and metallicity $Z = 0.008$ (solid black line). Models for $t > 5\,Gyr$ are from Paper I ($Z = 0.0001$ green three–pointed stars; and $Z = 0.001$ blue four–pointed stars). See the electronic edition of the Journal for a color version of the figure.

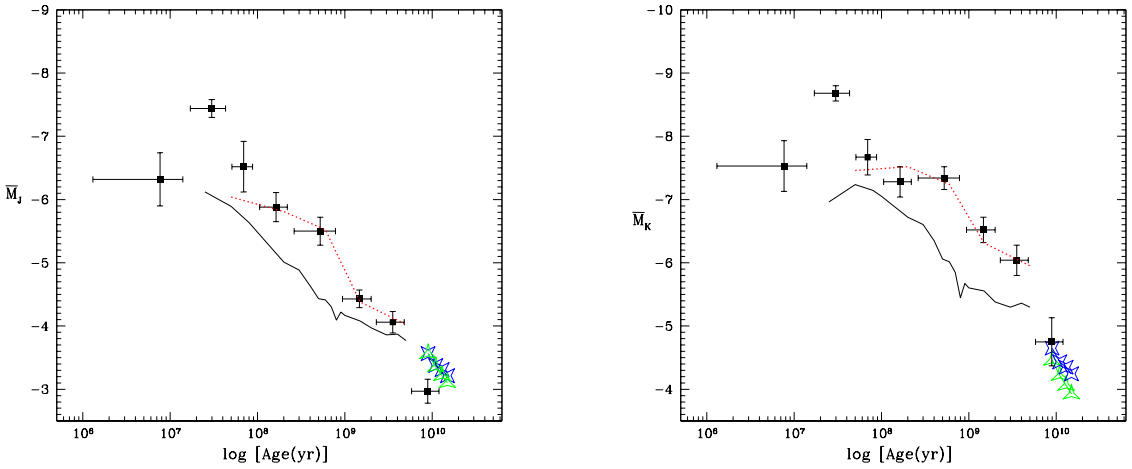

Fig. 12.— J– and K– SBF predictions for theoretical superclusters obtained from $B1$–models by including a contamination of M–type field stars *and* by artificially increasing the number of stars with $J - K \gtrsim 1.3 - 1.4$ (C–stars ?) in the SSPs (red dotted line). As reference original $B1$–models with $Z = 0.008$ are reported (black solid line). Symbols are as in Fig. 11. See the electronic edition of the Journal for a color version of the figure.

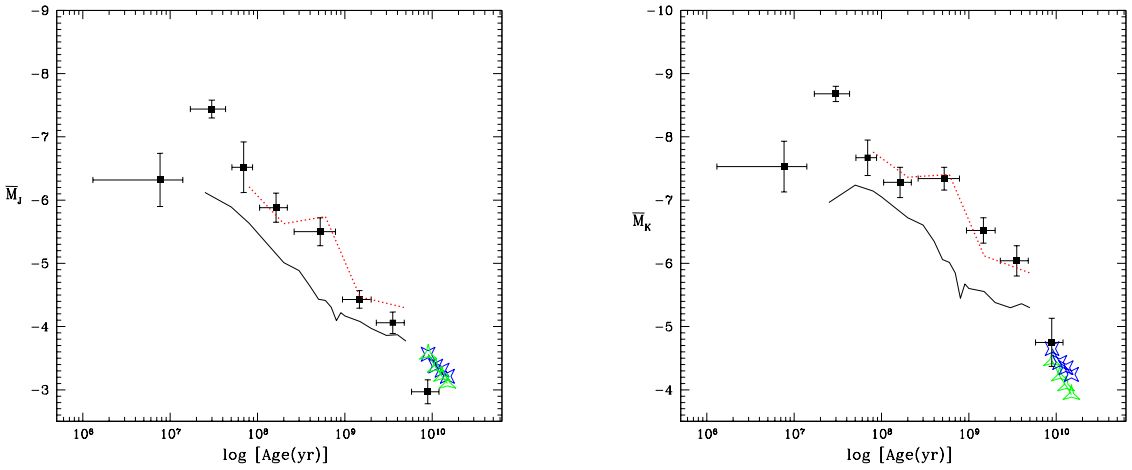

Fig. 13.— J– and K– SBF for composite stellar populations (red dotted line, see text). Symbols are as in Fig. 11. See the electronic edition of the Journal for a color version of the figure.

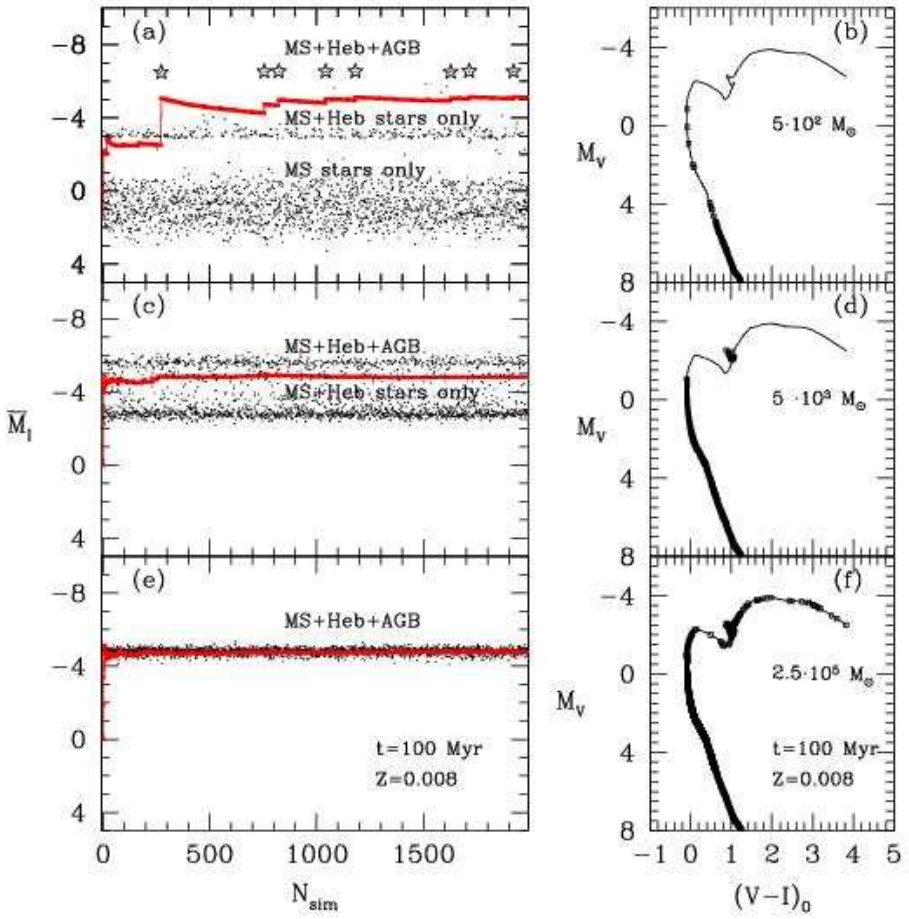

Fig. 14.— Left panels: $\overline{M_I}$ for a population of $100\,Myr$ and $Z = 0.008$ as function of the simulation number N_{sim}. The total mass of the stellar population increases from the top to the bottom: $\mathcal{M}_{tot} = 5{\cdot}10^2\ M_\odot$ (panel a); $\mathcal{M}_{tot} = 5{\cdot}10^3\ M_\odot$ (panel c); and $\mathcal{M}_{tot} = 2.5{\cdot}10^5\ M_\odot$ (panel e). The tick (red) solid lines refer to SBF computed from *std*–procedure. Differently, each dot represents the SBF as derived from the j–th synthetic CMD ($M_I^{RS,j}$, RS–procedure). In panel (a) the five–pointed stars at $\overline{M}_I^{RS,j} \sim -6.5\,mag$ enlighten the few simulations in which also a few AGB stars are occasionally present in the CMD. Right panels: the typical distribution of stars (squares) in the synthetic CMD for the labelled total mass, and the corresponding isochrone (solid line). Total masses are the same as in the corresponding left panels. See the electronic edition of the Journal for a color version of the figure.

Table 1. SBF amplitudes for $B1$–models

Age (Gyr)	$\bar{M}_U$	$\bar{M}_B$	$\bar{M}_V$	$\bar{M}_R$	$\bar{M}_I$	$\bar{M}_J$	$\bar{M}_H$	$\bar{M}_K$	$\bar{M}_L$	M_V^{Tot}	$V-I$
$Z = 0.0003$ $Y = 0.245$											
0.025	−3.901	−3.010	−2.759	−2.794	−2.929	−3.435	−4.147	−4.231	−4.404	−8.872	-0.092
0.030	−3.639	−2.764	−2.584	−2.811	−3.275	−4.434	−5.461	−5.575	−5.783	−8.783	-0.063
0.050	−3.018	−2.473	−3.528	−4.597	−5.551	−7.078	−8.007	−8.128	−8.304	−8.746	0.276
0.080	−2.441	−2.041	−3.013	−4.051	−5.006	−6.555	−7.547	−7.675	−7.863	−8.572	0.240
0.100	−2.171	−1.867	−2.855	−3.888	−4.839	−6.392	−7.393	−7.523	−7.713	−8.515	0.252
0.200	−1.450	−1.326	−2.303	−3.284	−4.192	−5.711	−6.718	−6.845	−7.042	−8.312	0.292
0.300	−1.011	−0.990	−1.900	−2.863	−3.766	−5.329	−6.385	−6.522	−6.726	−8.187	0.320
0.400	−0.645	−0.761	−1.503	−2.377	−3.232	−4.759	−5.822	−5.959	−6.170	−8.121	0.323
0.500	−0.295	−0.632	−1.393	−2.232	−3.058	−4.543	−5.598	−5.733	−5.943	−8.089	0.351
0.600	−0.098	−0.458	−1.300	−2.142	−2.948	−4.387	−5.414	−5.550	−5.751	−8.109	0.417
0.700	−0.022	−0.489	−1.411	−2.212	−2.967	−4.341	−5.330	−5.466	−5.660	−8.147	0.539
0.800	0.346	−0.136	−1.227	−2.004	−2.707	−3.904	−4.794	−4.910	−5.089	−7.888	0.595
0.900	0.411	−0.123	−1.386	−2.200	−2.915	−4.134	−5.046	−5.169	−5.346	−7.838	0.662
1.000	0.566	0.050	−1.217	−2.004	−2.689	−3.825	−4.682	−4.795	−4.965	−7.755	0.677
1.500	0.843	0.099	−1.334	−2.148	−2.830	−3.926	−4.750	−4.858	−5.017	−7.502	0.761
2.000	1.049	0.343	−1.061	−1.866	−2.544	−3.646	−4.478	−4.588	−4.749	−7.232	0.752
3.000	1.137	0.395	−1.000	−1.802	−2.473	−3.538	−4.344	−4.444	−4.597	−6.945	0.774
4.000	1.168	0.334	−1.077	−1.882	−2.555	−3.641	−4.452	−4.554	−4.708	−6.764	0.813
5.000	1.206	0.353	−1.033	−1.823	−2.485	−3.534	−4.325	−4.421	−4.569	−6.592	0.833
$Z = 0.001$ $Y = 0.246$											
0.025	−4.390	−3.844	−3.744	−3.844	−4.052	−4.739	−5.542	−5.669	−5.874	−9.366	-0.048
0.030	−4.128	−3.686	−3.599	−3.727	−4.001	−4.854	−5.764	−5.898	−6.114	−9.302	-0.014
0.050	−3.424	−3.079	−3.433	−4.176	−5.036	−6.762	−7.822	−7.979	−8.178	−9.186	0.267
0.080	−2.713	−2.484	−2.876	−3.599	−4.436	−6.154	−7.271	−7.438	−7.653	−8.987	0.269
0.100	−2.370	−2.182	−2.639	−3.400	−4.249	−5.973	−7.092	−7.261	−7.475	−8.894	0.299
0.200	−1.386	−1.469	−2.014	−2.815	−3.672	−5.429	−6.574	−6.747	−6.966	−8.574	0.366
0.300	−0.555	−0.943	−1.664	−2.500	−3.359	−5.116	−6.268	−6.440	−6.656	−8.364	0.410
0.400	−0.010	−0.486	−1.320	−2.131	−2.959	−4.694	−5.863	−6.039	−6.259	−8.191	0.432
0.500	0.319	−0.081	−1.062	−1.896	−2.720	−4.437	−5.603	−5.776	−5.997	−8.090	0.461
0.600	0.546	0.199	−0.933	−1.754	−2.533	−4.128	−5.240	−5.407	−5.621	−8.070	0.543
0.700	0.722	0.192	−1.172	−2.002	−2.742	−4.188	−5.226	−5.388	−5.583	−8.140	0.684
0.800	1.057	0.272	−1.255	−2.115	−2.860	−4.306	−5.321	−5.480	−5.668	−7.895	0.732
0.900	1.197	0.367	−1.170	−2.026	−2.763	−4.157	−5.147	−5.302	−5.487	−7.780	0.730
1.000	1.276	0.432	−1.101	−1.953	−2.681	−3.995	−4.929	−5.070	−5.248	−7.710	0.734
1.500	1.496	0.525	−1.038	−1.897	−2.625	−3.941	−4.865	−5.004	−5.181	−7.475	0.769
2.000	1.674	0.675	−0.890	−1.752	−2.479	−3.778	−4.686	−4.820	−4.994	−7.267	0.785
3.000	1.787	0.731	−0.813	−1.672	−2.399	−3.746	−4.674	−4.812	−4.989	−6.925	0.817
4.000	1.876	0.766	−0.769	−1.625	−2.353	−3.743	−4.696	−4.838	−5.017	−6.676	0.845
5.000	1.971	0.861	−0.655	−1.505	−2.230	−3.634	−4.594	−4.736	−4.916	−6.472	0.863
$Z = 0.004$ $Y = 0.251$											
0.025	−4.851	−4.708	−4.679	−4.840	−5.147	−5.962	−6.738	−6.865	−7.036	−10.077	0.206
0.030	−4.219	−4.134	−4.193	−4.482	−4.931	−5.839	−6.566	−6.678	−6.829	−9.854	0.342
0.050	−3.323	−3.402	−3.550	−3.974	−4.659	−6.273	−7.415	−7.637	−7.875	−9.562	0.427
0.080	−2.071	−2.482	−2.817	−3.308	−4.052	−5.784	−6.999	−7.249	−7.509	−9.238	0.462
0.100	−1.397	−1.835	−2.412	−3.013	−3.821	−5.615	−6.850	−7.103	−7.366	−9.059	0.503
0.200	0.007	−0.109	−1.234	−2.129	−3.150	−5.163	−6.459	−6.723	−6.990	−8.525	0.553
0.300	0.487	0.355	−0.802	−1.711	−2.746	−4.817	−6.161	−6.439	−6.718	−8.287	0.537
0.400	1.070	0.853	−0.546	−1.605	−2.731	−4.818	−6.132	−6.388	−6.647	−8.070	0.561
0.500	1.436	1.175	−0.254	−1.335	−2.473	−4.592	−5.916	−6.180	−6.444	−7.918	0.574
0.600	1.708	1.303	−0.202	−1.277	−2.344	−4.276	−5.518	−5.744	−5.980	−7.835	0.598
0.700	1.807	1.096	−0.510	−1.516	−2.471	−4.190	−5.336	−5.547	−5.769	−7.895	0.695
0.800	1.852	0.971	−0.685	−1.679	−2.607	−4.270	−5.379	−5.585	−5.801	−7.952	0.763
0.900	2.027	1.066	−0.640	−1.658	−2.616	−4.348	−5.476	−5.690	−5.918	−7.665	0.764
1.000	2.120	1.127	−0.575	−1.587	−2.523	−4.187	−5.277	−5.476	−5.690	−7.569	0.760
1.500	2.477	1.291	−0.431	−1.441	−2.373	−4.032	−5.115	−5.310	−5.521	−7.273	0.802
2.000	2.615	1.320	−0.375	−1.370	−2.315	−4.021	−5.125	−5.328	−5.545	−7.122	0.866
3.000	2.789	1.441	−0.232	−1.228	−2.194	−3.929	−5.041	−5.244	−5.458	−6.775	0.918
4.000	2.900	1.478	−0.184	−1.174	−2.145	−3.886	−4.997	−5.198	−5.411	−6.497	0.945
5.000	2.977	1.583	−0.052	−1.042	−2.037	−3.829	−4.958	−5.163	−5.379	−6.279	0.962
$Z = 0.008$ $Y = 0.256$											
0.025	−4.259	−4.523	−4.596	−4.841	−5.259	−6.121	−6.835	−6.963	−7.119	−10.214	0.445
0.050	−1.598	−1.556	−2.816	−3.630	−4.521	−5.892	−6.959	−7.236	−7.548	−9.402	0.674
0.080	−0.855	−0.641	−1.906	−2.839	−3.994	−5.634	−6.840	−7.144	−7.483	−9.058	0.643
0.100	−0.561	−0.386	−1.597	−2.532	−3.756	−5.483	−6.739	−7.051	−7.398	−8.912	0.610
0.200	0.126	0.193	−0.757	−1.681	−3.083	−5.012	−6.384	−6.722	−7.092	−8.497	0.539
0.300	0.843	0.814	−0.262	−1.331	−2.903	−4.886	−6.273	−6.605	−6.966	−8.221	0.560

Table 1—Continued

Age (Gyr)	$\bar{M}_U$	$\bar{M}_B$	$\bar{M}_V$	$\bar{M}_R$	$\bar{M}_I$	$\bar{M}_J$	$\bar{M}_H$	$\bar{M}_K$	$\bar{M}_L$	M_V^{Tot}	$V-I$
0.400	1.332	1.209	0.110	−1.028	−2.658	−4.638	−6.027	−6.348	−6.701	−8.008	0.566
0.500	1.680	1.432	0.206	−0.985	−2.543	−4.433	−5.767	−6.058	−6.381	−7.873	0.600
0.600	1.962	1.578	0.203	−1.016	−2.548	−4.412	−5.728	−6.017	−6.338	−7.769	0.635
0.700	2.147	1.543	0.018	−1.141	−2.543	−4.307	−5.569	−5.850	−6.164	−7.773	0.722
0.800	2.273	1.426	−0.225	−1.338	−2.528	−4.096	−5.218	−5.448	−5.700	−7.806	0.796
0.900	2.377	1.486	−0.178	−1.297	−2.572	−4.221	−5.407	−5.673	−5.978	−7.522	0.803
1.000	2.491	1.553	−0.127	−1.253	−2.530	−4.170	−5.345	−5.603	−5.901	−7.443	0.822
1.500	2.903	1.721	0.016	−1.097	−2.411	−4.081	−5.276	−5.554	−5.870	−7.113	0.898
2.000	3.142	1.817	0.089	−1.034	−2.358	−3.970	−5.132	−5.382	−5.667	−6.895	0.953
3.000	3.357	1.962	0.276	−0.839	−2.232	−3.862	−5.043	−5.298	−5.594	−6.573	1.013
4.000	3.503	2.056	0.398	−0.712	−2.181	−3.871	−5.085	−5.363	−5.683	−6.317	1.050
5.000	3.659	2.197	0.554	−0.548	−2.048	−3.773	−5.010	−5.298	−5.630	−6.080	1.062
$Z = 0.01$ $Y = 0.259$											
0.025	−4.220	−3.903	−3.978	−4.386	−4.994	−6.064	−6.851	−6.991	−7.149	−9.914	0.416
0.030	−3.775	−3.848	−3.987	−4.342	−4.877	−5.854	−6.618	−6.755	−6.911	−9.882	0.464
0.050	−1.542	−1.176	−2.485	−3.417	−4.403	−5.884	−6.969	−7.283	−7.602	−9.346	0.682
0.080	−0.910	−0.585	−1.755	−2.697	−3.884	−5.612	−6.823	−7.169	−7.515	−9.043	0.621
0.100	−0.627	−0.419	−1.534	−2.454	−3.709	−5.505	−6.760	−7.109	−7.457	−8.920	0.592
0.200	0.191	0.257	−0.680	−1.600	−3.040	−5.059	−6.432	−6.807	−7.177	−8.498	0.531
0.300	0.894	0.909	−0.010	−1.050	−2.703	−4.809	−6.207	−6.577	−6.944	−8.189	0.542
0.400	1.365	1.260	0.297	−0.838	−2.594	−4.660	−6.045	−6.395	−6.747	−7.975	0.558
0.500	1.708	1.446	0.187	−1.073	−2.722	−4.618	−5.919	−6.232	−6.550	−7.843	0.614
0.600	2.023	1.628	0.261	−1.007	−2.658	−4.545	−5.843	−6.158	−6.478	−7.744	0.653
0.700	2.222	1.567	0.015	−1.154	−2.567	−4.277	−5.490	−5.782	−6.082	−7.765	0.756
0.800	2.347	1.482	−0.167	−1.304	−2.624	−4.274	−5.448	−5.739	−6.039	−7.796	0.846
0.900	2.473	1.572	−0.117	−1.292	−2.665	−4.314	−5.475	−5.754	−6.047	−7.511	0.854
1.000	2.590	1.683	−0.002	−1.179	−2.566	−4.222	−5.390	−5.670	−5.964	−7.400	0.859
1.500	3.032	1.877	0.171	−0.974	−2.382	−4.085	−5.275	−5.578	−5.890	−7.037	0.927
2.000	3.317	1.998	0.273	−0.873	−2.319	−4.034	−5.226	−5.530	−5.843	−6.812	0.982
3.000	3.569	2.132	0.434	−0.698	−2.193	−3.943	−5.144	−5.452	−5.772	−6.504	1.046
4.000	3.688	2.241	0.580	−0.543	−2.072	−3.809	−5.013	−5.310	−5.623	−6.240	1.077
5.000	3.798	2.284	0.637	−0.474	−2.022	−3.826	−5.047	−5.366	−5.695	−6.035	1.103
$Z = 0.0198$ $Y = 0.273$											
0.025	−4.341	−4.161	−4.143	−4.356	−4.902	−5.894	−6.777	−6.961	−7.123	−10.042	0.318
0.050	−2.683	−2.920	−3.080	−3.409	−4.134	−5.968	−7.145	−7.626	−7.970	−9.545	0.417
0.080	−1.435	−1.423	−2.031	−2.609	−3.571	−5.775	−7.021	−7.521	−7.871	−9.172	0.458
0.100	−0.887	−0.696	−1.442	−2.175	−3.291	−5.655	−6.925	−7.441	−7.800	−8.979	0.492
0.200	0.237	0.388	−0.171	−1.024	−2.530	−5.271	−6.587	−7.098	−7.456	−8.433	0.488
0.300	0.937	0.911	0.291	−0.669	−2.396	−5.087	−6.387	−6.859	−7.192	−8.134	0.533
0.400	1.418	1.270	0.500	−0.567	−2.432	−4.957	−6.232	−6.681	−7.000	−7.915	0.587
0.500	1.826	1.585	0.692	−0.435	−2.326	−4.719	−5.983	−6.419	−6.731	−7.754	0.632
0.600	2.136	1.778	0.680	−0.490	−2.334	−4.656	−5.899	−6.330	−6.639	−7.644	0.689
0.700	2.435	1.890	0.487	−0.700	−2.309	−4.380	−5.564	−5.976	−6.273	−7.628	0.813
0.800	2.619	1.939	0.444	−0.739	−2.333	−4.350	−5.519	−5.933	−6.230	−7.594	0.883
0.900	2.739	1.997	0.422	−0.792	−2.432	−4.526	−5.673	−6.086	−6.379	−7.358	0.944
1.000	2.869	2.075	0.453	−0.761	−2.381	−4.429	−5.575	−5.984	−6.276	−7.225	0.949
1.500	3.382	2.385	0.702	−0.497	−2.131	−4.243	−5.391	−5.791	−6.076	−6.817	1.007
2.000	3.770	2.547	0.838	−0.335	−1.930	−4.077	−5.231	−5.639	−5.927	−6.574	1.049
3.000	4.109	2.686	0.971	−0.204	−1.849	−4.135	−5.289	−5.713	−6.010	−6.256	1.101
4.000	4.250	2.722	1.049	−0.079	−1.651	−4.029	−5.187	−5.632	−5.939	−6.024	1.137
5.000	4.396	2.840	1.177	0.051	−1.548	−4.040	−5.192	−5.639	−5.943	−5.817	1.174
$Z = 0.04$ $Y = 0.30$											
0.025	−3.985	−4.192	−4.247	−4.393	−4.800	−5.750	−6.630	−6.870	−7.058	−10.056	0.305
0.030	−3.390	−3.752	−3.931	−4.142	−4.664	−6.723	−7.857	−8.348	−8.671	−9.936	0.374
0.050	−1.901	−1.692	−2.450	−3.089	−3.875	−6.023	−7.214	−7.785	−8.173	−9.413	0.490
0.080	−1.166	−0.690	−1.206	−1.999	−3.076	−5.728	−6.952	−7.529	−7.915	−8.996	0.498
0.100	−0.828	−0.401	−0.796	−1.548	−2.698	−5.627	−6.890	−7.489	−7.884	−8.831	0.479
0.200	0.259	0.368	0.099	−0.580	−1.934	−5.302	−6.621	−7.230	−7.628	−8.329	0.474
0.300	0.954	0.914	0.560	−0.170	−1.602	−5.143	−6.456	−7.048	−7.431	−8.015	0.533
0.400	1.549	1.363	0.840	0.043	−1.590	−5.037	−6.322	−6.878	−7.243	−7.785	0.596
0.500	1.972	1.717	1.030	0.147	−1.616	−4.866	−6.127	−6.661	−7.016	−7.607	0.653
0.600	2.319	2.016	1.147	0.201	−1.576	−4.726	−5.974	−6.501	−6.850	−7.461	0.709
0.700	2.594	2.249	1.156	0.100	−1.801	−4.996	−6.188	−6.693	−7.026	−7.328	0.807
0.800	2.727	2.400	1.188	0.030	−1.607	−4.557	−5.768	−6.285	−6.625	−6.919	0.775
0.900	2.915	2.556	1.232	0.020	−1.698	−4.488	−5.674	−6.171	−6.498	−6.811	0.833
1.000	3.104	2.646	1.225	−0.001	−1.744	−4.505	−5.676	−6.166	−6.492	−6.718	0.878
1.500	3.695	2.746	1.158	0.030	−1.572	−4.316	−5.463	−5.956	−6.282	−6.585	1.044

Table 1—Continued

Age (Gyr)	$\bar{M}_U$	$\bar{M}_B$	$\bar{M}_V$	$\bar{M}_R$	$\bar{M}_I$	$\bar{M}_J$	$\bar{M}_H$	$\bar{M}_K$	$\bar{M}_L$	M_V^{Tot}	$V-I$
2.000	4.063	2.851	1.232	0.120	−1.467	−4.218	−5.358	−5.845	−6.163	−6.334	1.089
3.000	4.466	3.051	1.422	0.330	−1.224	−4.136	−5.286	−5.795	−6.123	−5.992	1.135
4.000	4.662	3.166	1.546	0.461	−1.094	−4.078	−5.230	−5.744	−6.077	−5.761	1.158
5.000	4.796	3.245	1.633	0.558	−0.979	−3.999	−5.152	−5.674	−6.012	−5.590	1.183

Table 2. Overview of the WFPC2 observations for young clusters in the sample.

Cluster	Archive Directory/File	Filter	Total Exp. time (sec)	Date (DD/MM/YY)
NGC 1805	u4ax0204b	F555W	435	25/07/1998
	u4ax020ab	F814W	960	25/07/1998
	u4ax0501b	F555W	7200	12/03/1998
	u4ax0601b	F814W	4800	12/03/1998
	u4ax0803b	F555W	2500	29/04/1998
	u4ax0903b	F814W	2500	28/04/1998
NGC 1818	u4ax3004b	F555W	435	25/09/1998
	u4ax300ab	F814W	960	25/09/1998
	u4ax3301b	F555W	7200	11/07/1998
	u4ax3501b	F814W	4800	29/07/1998
	u4ax3603b	F555W	2500	30/04/1998
	u4ax3703b	F814W	2500	30/04/1998
NGC 1868	u4ax5204b	F555W	435	12/11/1998
	u4ax520ab	F814W	960	12/11/1998
	u4ax5301b	F555W	7200	21/03/1998
	u4ax5601b	F814W	4800	22/03/1998
	u4ax5803b	F555W	2500	20/05/1998
	u4ax5903b	F814W	2500	24/05/1998
NGC 1831	u4ax4104b	F555W	435	25/07/1998
	u4ax410ab	F814W	960	25/07/1998
	u4ax4401b	F555W	7200	24/07/1998
	u4ax4601b	F814W	4800	24/07/1998
	u4ax4703b	F555W	2500	29/05/1998
	u4ax4803b	F814W	2500	30/05/1998
NGC 2209	u4ax6304b	F555W	435	29/03/1998
	u4ax630ab	F814W	960	29/03/1998
	u4ax6401b	F555W	7200	28/03/1998
	u4ax6701b	F814W	4800	03/04/1998
	u4ax6903b	F555W	2500	06/05/1998
	u4ax7003b	F814W	2500	05/05/1998
H14	u4ax7404b	F555W	435	31/03/1998
	u4ax740ab	F814W	960	31/03/1998
	u4ax7301b	F555W	1200	04/02/1998
	u4ax7303b	F814W	800	04/02/1998
	u4ax7501b	F555W	7200	06/08/1998
	u4ax7801b	F814W	4800	05/08/1998

Table 3. Clusters properties and measured SBF

NGC	V_{tot}[a]	V_{tot}	$\bar{V}$	$\bar{I}$	$\bar{V}-\bar{I}$	log [t(yr)]	Ref.
1805	10.63	10.9	15.31±0.2	15.30±0.2	0.01±0.3	$7.00^{+0.30}_{-0.10}$	2
1818	9.70	10.2	15.00±1.0	14.37±1.0	0.63±1.0	7.40±0.30	1
1866	9.73	9.4	17.09±0.2	14.95±0.2	2.14±0.07	8.15± 0.30	3
1831	11.18	10.9	18.47±0.2	15.90±0.2	2.57±0.3	8.65± 0.30	1
1868	11.56	11.5	18.68±0.5	16.50±0.5	2.18±0.5	8.81± 0.30	1
2209	13.15	12.5	18.75±0.5	16.66±0.5	2.09±0.5	8.85± 0.20	1
$Hodge14$	11.45	13.7	19.21±1.0	17.29±1.0	1.92±0.5	9.30± 0.10	1
1754	11.86	12.2	18.42±0.5	16.70±0.5	1.72±0.4	$10.19^{+0.06}_{-0.07}$	2
1916	10.38	10.9	18.10±0.5	16.28±0.5	1.83±0.4	10.20±0.09	2
2005	11.57	11.7	18.18±0.5	16.11±0.5	2.07±0.4	$10.22^{+0.12}_{-0.16}$	2
2019	10.86	11.4	17.94±0.5	16.13±0.5	1.81±0.4	$10.25^{+0.07}_{-0.09}$	2

Note. — References for the cluster age: 1=present work; 2=MG03; 3=Brocato et al. (2003)

[a]Van den Bergh (1981)

Table A.1. Comparison with previous works. BH mass–loss rate is adopted.

$No.$	$m/M_\odot$	$m_c/M_\odot$	$L/L_\odot$
Present procedure (case a)			
1	6.928	0.938	33798
10	6.903	0.944	48265
20	6.837	0.953	64887
30	6.674	0.961	73937
Present procedure (case b)			
1	6.871	0.913	25217
10	6.848	0.920	36581
20	6.796	0.930	48570
30	6.728	0.940	54352
BS91			
1	6.871	0.913	25217
10	6.854	0.921	40268
20	6.821	0.930	51662
30	6.774	0.939	58806
Marigo (1998)			
1	6.871	0.913	25217
11	6.850	0.921	37788
22	6.807	0.930	51537
34	6.745	0.939	60760